Dalton Transactions

ROYAL SOCIETY OF CHEMISTRY

PAPER

View Article Online
View Journal | View Issue

Check for updates

Cite this: *Dalton Trans.*, 2025, **54**, 14821

Manganese germylene hydride complexes: reactivity with carbon dioxide, benzophenone, and diisopropylcarbodiimide

Jeffrey S. Price and David J. H. Emslie *

Reactions of bis(hydrocarbyl)germylene manganese(I) hydride complexes [(dmpe)$_2$MnH(=GeR$_2$)] (**1a**: R = Ph, **1b**: R = Et) with carbon dioxide yielded the previously reported carbonyl formate complex [(dmpe)$_2$Mn(κ^1-O$_2$CH)(CO)] (**3**) *via* the unstable κ^2-formatogermyl intermediates [(dmpe)$_2$Mn{κ^2-GeR$_2$(OCHO)}] (**5a**: R = Ph, **5b**: R = Et). By contrast, addition of CO$_2$ to [(dmpe)$_2$MnH(=Ge^{n}BuH)] (**2a**), which contains a terminal GeH substitutent, resulted in the sequential formation of (i) the formatogermylene hydride complex [(dmpe)$_2$MnH{=Ge^{n}Bu(κ^1-O$_2$CH)}] (**6**), (ii) the isolable metallacyclic κ^2-formatogermyl complex [(dmpe)$_2$Mn{κ^2-Ge^{n}Bu(κ^1-O$_2$CH)(OCHO)}] (**7**), and with heating(III) complex **3**. Exposure of **2a** to benzophenone also afforded a new germylene hydride complex, [(dmpe)$_2$MnH{=Ge^{n}Bu(OCHPh$_2$)}] (**8**). Reactions of **1a–b** and **2a** with C(N^{i}Pr)$_2$ afforded a family of stable metallacyclic κ^2-amidinylgermyl complexes [(dmpe)$_2$Mn{κ^2-GeRR′(N^{i}PrCHN^{i}Pr)}] (**9a**: R = R′ = Ph, **9b**: R = R′ = Et, **10**: R = ^{n}Bu and R′ = H). Addition of carbon dioxide to **10** yielded [(dmpe)$_2$Mn{κ^2-Ge^{n}Bu(κ^1-O$_2$CH)(N^{i}PrCHN^{i}Pr)}] (**11**), and reaction of CO$_2$ with the κ^2-amidinylsilyl derivative [(dmpe)$_2$Mn{κ^2-SiPhH(N^{i}PrCHN^{i}Pr)}] afforded [(dmpe)$_2$Mn{κ^2-SiPh(κ^1-O$_2$CH)(N^{i}PrCHN^{i}Pr)}] (**12**). Complexes **6**, **7**, **8**, **9a**, **11**, and **12** were crystallographically characterized, and DFT calculations were conducted to probe the effect that different substituents on Ge have on Mn–Ge bonding in κ^2-formatogermyl, κ^2-amidinylgermyl, and germylene complexes.

Received 18th July 2025,
Accepted 1st September 2025

DOI: 10.1039/d5dt01701g

rsc.li/dalton

Introduction

Small molecule activation of carbon dioxide is of great interest given that CO$_2$ is a widely available and inexpensive C1 synthon.[1–6] Thus, catalytic and stoichiometric CO$_2$ activation by transition metal complexes has become an area of intense and growing focus.[7–11] Germylenes (GeR$_2$), which feature low valent and (often) sterically accessible Ge centres, offer an intriguing platform for carbon dioxide reactivity. Over the past two decades, examples have been reported involving CO$_2$ insertion into a Ge–H bond to afford formate-substituted germylenes (Scheme 1(a)),[12–14] oxo-transfer reactions (Scheme 1(b)),[15] and CO$_2$ incorporation into larger substituents on Ge (Scheme 1(c)).[16] Free H-substituted germylenes (R$_2$NGeH or (BDI)GeH; BDI = β-diketiminate) have also demonstrated activity for catalytic reduction of CO$_2$ [17] and have been the subject of computational reports on catalytic CO$_2$ hydroboration.[18] Furthermore, an oxo-transfer reaction from CO$_2$ to (BDI)Ga(μ-Cl)GeAr (Ar = 2,6-dimesitylphenyl) has recently been described,[19] and Frustrated Lewis Pair reactivity has been

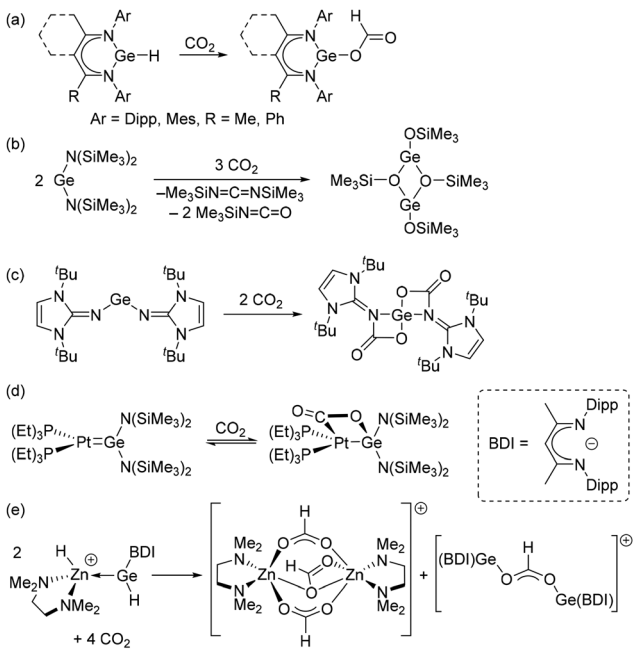

Scheme 1 Literature examples of CO$_2$ reactivity with free germylenes (a–c) and d-block germylene complexes (d and e).[12–16,21,22]

Department of Chemistry, McMaster University, 1280 Main St. West, Hamilton, Ontario, L8S 4M1, Canada. E-mail: emslied@mcmaster.ca

demonstrated involving a free germylene and a cyclic (alkyl)(amino)carbene (cAAC).[20]

By contrast, the reactivity of carbon dioxide with d-block germylene complexes (which often contain germylene ligands which would be unstable outside of the metal's coordination sphere)[23] remains relatively unexplored. To our knowledge, the only reported examples involve a platinum germylene complex which undergoes reversible cycloaddition with carbon dioxide (Scheme 1(d))[21] and a zinc germylene species where CO_2 insertion into both Ge–H and Zn–H bonds was observed[22] (Scheme 1(e)).

Expanding the scope to reactions of transition metal germylene complexes with other organic reagents containing unsaturated C=O bonds, ketones and aldehydes have been shown to form hydrogermylation products upon reaction with the hydridogermylene hydride complexes $[Cp^*(OC)_nMH(=GeH\{C(SiMe_3)_3\})]$ (M = W and n = 2,[24] or M = Fe and n = 1;[25] Scheme 2). These reactions were suggested to proceed *via* (i) initial ketone/aldehyde coordination to Ge, (ii) 1,4-H transfer of the metal hydride to the carbonyl C atom, affording a germyl intermediate, and (iii) 1,2-H migration of the GeH substituent onto the metal to afford the germylene product.[24,25] In addition, the acetylide–germylene complexes $[Cp^*(OC)_2W(=GePh_2)(C{\equiv}CEMe_3)]$ (E = C, Si) were found to undergo cycloaddition with acetone to afford 6-membered metallacyclic vinylidene complexes (Scheme 2).[26]

Reactions of transition metal germylene complexes with nitriles,[24,25,27] isocyanates,[25,27–29] and isothiocyanates,[25,28] all of which feature unsaturated C–N bonds, have also been reported. While insertion of carbodiimides $\{C(NR)_2\}$, which are isoelectronic with CO_2, into a Ge–N bond in the free germylene $Ge\{N(Me_2SiCH_2)_2\}_2$ [30] or the Ge–Ga bond in the gallium-substituted germylene $[(BDI)Ga(\mu\text{-}Cl)GeAr]$[19] have been reported, to the best of our knowledge, reactions between a transition metal-coordinated germylene and a carbodiimide have not yet been published.

Our group recently reported the synthesis of diorganylgermylene manganese(I) hydride complexes $[(dmpe)_2MnH(=GeRR')]$ (**1a**: R = R′ = Ph, **1b**: R = R′ = Et, **2a**: R = ^{n}Bu and R′ = H, **2b**: R = Ph and R′ = H; only **1a–b** and **2a** were isolated with analytical purity),[31] as a natural outgrowth of our investigations into the synthesis and reactivity of their lighter silylene congeners $[(dmpe)_2MnH(=SiR_2)]$ (R = Ph, Et) and the related disilyl hydride complexes $[(dmpe)_2MnH(SiH_2R)_2]$ (R = Ph, ^{n}Bu; in solution, these species exist in equilibrium with silylene hydride complexes $[(dmpe)_2MnH(=SiRH)]$).[32–36] Reactions between these silicon-containing compounds and carbon dioxide afforded the manganese(I) formate complex $[(dmpe)_2Mn(\kappa^1\text{-}O_2CH)(CO)]$ (**3**) and siloxane by-products; Scheme 3.[36] We also demonstrated that diisopropylcarbodiimide $\{C(N^iPr)_2\}$ reacts with the same silicon-containing reagents to afford the metallacyclic κ^2-amidinylsilyl complexes $[(dmpe)_2Mn\{\kappa^2\text{-}SiRR'(N^iPrCHN^iPr)\}]$ (Scheme 3).[36]

The reactions of these manganese silylene and disilyl hydride complexes with CO_2 (Scheme 3) were proposed to proceed *via* a multi-step mechanism to form the carbonyl hydride complex $[(dmpe)_2MnH(CO)]$ (**4**), which then undergoes reversible CO_2 insertion into the Mn–H bond to afford **3**.[36] In this reaction, one equivalent of CO_2 was reduced to CO, presumably driven by energetically favourable Si–O bond formation. Using germylene derivatives in place of the silylene complexes would reduce the thermodynamic driving force for such reactivity given the lower bond energy of Ge–O *versus* Si–O bonds,[37] potentially permitting isolation and/or observation of reaction intermediates, providing greater insight into CO_2 activation by transition metal tetrylene complexes.

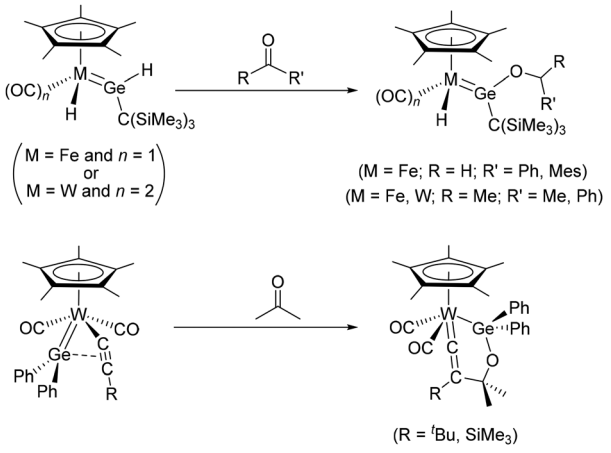

Scheme 2 Literature reactions of ketones and aldehydes with transition metal germylene complexes.[24–26] Interligand interactions between germylene and hydride ligands are not shown (in the top reaction, the W starting material features such an interaction, while the Fe starting material does not).

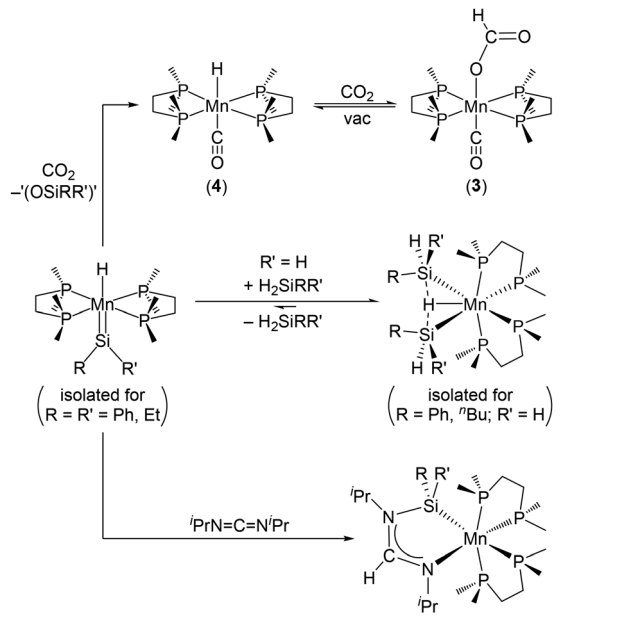

Scheme 3 Reactions of silylene hydride complexes $[(dmpe)_2MnH(=SiR_2)]$ (R = Ph, Et; only one isomer is shown) and disilyl hydride complexes $[(dmpe)_2MnH(SiH_2R)_2]$ (R = Ph, ^{n}Bu) with CO_2 and $C(N^iPr)_2$.

Results and discussion

Reactions of germylene hydride complexes with CO_2

Reactions of the bis(hydrocarbyl)germylene manganese(I) hydride complexes [(dmpe)$_2$MnH(=GeR$_2$)] (**1a**: R = Ph, **1b**: R = Et) with carbon dioxide resulted in solution colour changes from dark bronze to bright red (within 1–2 h), and then to pale yellow (within 2 d). The germylene starting materials were consumed within 2 hours at room temperature,† affording unstable [(dmpe)$_2$Mn{κ^2-GeR$_2$(OCHO)}] (**5a**: R = Ph, **5b**: R = Et; Scheme 4) complexes. These intermediary products converted over several days to the manganese(I) carbonyl formate complex [(dmpe)$_2$Mn(κ^1-O$_2$CH)(CO)] (**3**) accompanied by germanium-containing byproducts (Scheme 4). Complex **3** was also formed, along with siloxane byproducts, in previously reported reactions of [(dmpe)$_2$MnH(=SiR$_2$)] or [(dmpe)$_2$MnH(SiH$_2$R)$_2$] with CO_2. However, these reactions proceeded rapidly at room temperature, and while silicon analogues of **5a–b** were proposed as potential intermediates, they were not observed.[36] In the absence of CO_2, intermediate **5a** (which was investigated due to greater stability relative to **5b**) decomposed to afford previously reported [(dmpe)$_2$MnH(CO)] (**4**)[38] as the major product.

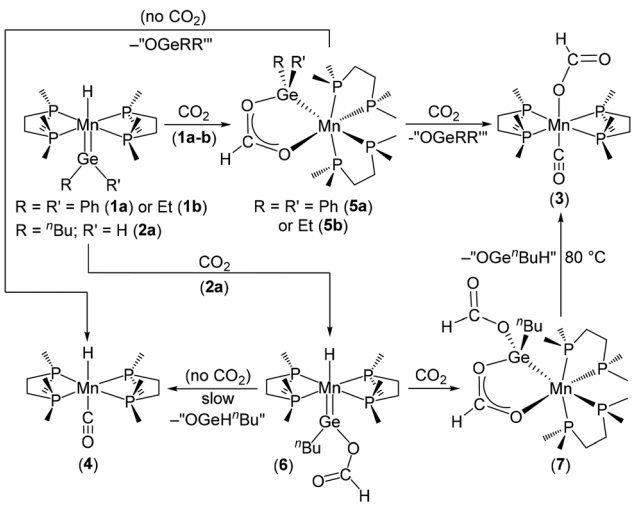

Scheme 4 Reactions of diorganylgermylene manganese(I) hydride complexes [(dmpe)$_2$MnH(=GeRR′)] (**1a**: R = R′ = Ph, **1b**: R = R′ = Et, **2a**: R = ^{n}Bu and R′ = H) with carbon dioxide. Only one diastereomer is shown for complex **7**. Compounds **5a–b** were not isolated; their structures are proposed based on *in situ* NMR spectroscopy, the preference of manganese(I) for a coordination number of six, DFT calculations, and the structure of an isolated κ^2-formatogermyl complex (**7**). Conversion of **5a–b** to **4** in the absence of carbon dioxide was only demonstrated for the more stable intermediate **5a**, and unidentified impurities were also formed. Note: **4** has previously been shown to reversibly insert CO_2 to yield formate complex **3**.[36]

The [(dmpe)$_2$Mn{κ^2-GeR$_2$(OCHO)}] (**5a**: R = Ph, **5b**: R = Et) intermediates gave rise to a high frequency singlet in the ^{1}H NMR spectra (**5a**: 8.1 ppm, **5b**: 7.8 ppm), suggestive of a formate group, and multiple ^{31}P NMR environments indicative of disphenoidal dmpe coordination. For the slightly more stable diphenyl derivative **5a**, further NMR characterization was conducted at −32 °C to limit decomposition. Additional NMR features include a high frequency formate environment in the ^{13}C{^{1}H} NMR spectrum at 172.7 ppm, two unique sets of phenyl signals indicative of diastereotopic GeR$_2$ substituents, and a lack of any low frequency (hydridic) ^{1}H NMR signal. While an X-ray crystal structure was not obtained for **5a–b**, κ^2*GeO*-coordination of the GeR$_2$(OCHO) ligand is proposed based on (a) the preference of manganese(I) for an octahedral coordination environment, affording an 18-electron species, (b) computational support (these structures were the lowest energy minima located by DFT calculations), and (c) the X-ray crystal structure and comparable spectroscopic features of an isolated κ^2-formatogermyl complex (**7**; *vide infra*).

Previously reported reactions of the germylene hydride complexes [Cp*(OC)$_n$MH(=GeH{C(SiMe$_3$)$_3$})] (M = W and n = 2, or M = Fe and n = 1) with ketones and aldehydes (Scheme 2) were proposed to proceed *via* initial coordination of the carbonyl substrate to germanium followed by 1,4-H transfer of the metal hydride to the *C*=O carbon atom.[26,27] Similar reactivity seems likely for the formation of **5a–b** from **1a–b** (where the final step involves coordination of the pendent oxygen to Mn, rather than α-hydride migration as observed in reactions with [Cp*(OC)$_n$MH(=GeH{C(SiMe$_3$)$_3$})]). However, a much broader range of mechanisms have been proposed for reactions of related silylene hydride complexes with unsaturated substrates,[36] and alternative pathways are plausible in this work (see SI including Scheme S1 for details).‡

While reactions of bis(hydrocarbyl)germylene manganese(I) hydride complexes **1a–b** with CO_2 ultimately afforded **3** at ambient temperature, analogous reactivity involving [(dmpe)$_2$MnH(=Ge^{n}BuH)] (**2a**), which features a terminal GeH substituent, required elevated temperature to generate the same carbonyl formate species **3**. At room temperature **2a** reacted with CO_2 to generate a new germylene hydride complex, [(dmpe)$_2$MnH{=Ge^{n}Bu(κ^1-O$_2$CH)}] (**6**), with a terminal formate substituent on germanium (Scheme 4). This complex is potentially formed *via* a mechanism analogous to that for the formation of **5a–b**, followed by α-H migration from Ge to Mn (Scheme S1). Direct insertion of CO_2 into the Ge–H

† For the reaction of **1b** with CO_2, another short lived intermediate with a ^{1}H NMR singlet at 8.77 ppm (and no corresponding hydride environment) was observed, but had been fully consumed within 30 minutes.

‡ Alternative mechanisms for the reactions of germylene hydride complexes with CO_2 could involve initial isomerization to a low-coordinate germyl isomer [(dmpe)$_2$Mn(GeHRR′)]. These species have been shown to exist in equilibrium with **1a–b** or **2a–b** by trapping with isonitriles, hydrogermanes, or N_2, along with reactions with D_2.[31,63] Isostructural primary germyl isonitrile complexes [(dmpe)$_2$Mn(GeH$_2$R)(CN^{t}Bu)] (**13a**: R = ^{n}Bu, **13b**: R = Ph) were prepared in this work by addition of free isonitriles to equilibrium mixtures of free hydrogermanes and germylene hydride complexes **2a–b**, along with the products of hydrogermane addition to **2a–b** (*trans*-[(dmpe)$_2$Mn(GeH$_2$R)(HGeH$_2$R)] and *mer*-[(dmpe)$_2$MnH(GeH$_2$R)$_2$]). X-ray crystal structures were obtained for ***cis*-13a** and both the *cis* and *trans* isomers of **13b** (Fig. S165).

bond of **2a** (similar to that proposed for alkene or alkyne reactivity with $[Cp^*(^iPr_3P)RuH_2(=GeHTrip)]^+$)[39] is unlikely given that this type of reactivity requires a highly electrophilic tetrylene center and is typically only observed in cationic complexes.[40,41]

Attempts to isolate a bulk sample of the formatogermylene hydride complex $[(dmpe)_2MnH\{=Ge^nBu(\kappa^1\text{-}O_2CH)\}]$ (**6**) were unsuccessful, and it was analysed *in situ* by NMR spectroscopy. The ^{1}H NMR spectrum of **6** includes a low frequency Mn*H* signal (−11.8 ppm; a quintet with $^2J_{H,P}$ of 53 Hz) and a high frequency formate (8.8 ppm) resonance, and one singlet was observed in the $^{31}P\{^1H\}$ NMR spectrum at 78 ppm, indicative of equatorial dmpe coordination to Mn(I). The observation of a single ^{31}P environment in compound **6** (and **2a–b**) by NMR spectroscopy is indicative of a rapid fluxional process (*e.g.* rapid phosphine dissociation and re-coordination). X-ray quality crystals of **6** were obtained from $O(SiMe_3)_2$ at −30 °C (Fig. 1; left), revealing an octahedral environment with *trans*-disposed germylene and hydride ligands. As expected for a base-free germylene complex, the germanium environment is planar (Σ(X–Ge–Y) = 359.8(3)°) and the Mn–Ge distance of 2.201(1) Å is significantly shorter than in manganese(I) germyl complexes {Mn–Ge = 2.29–2.47 Å for GeX_3 (X = halide or H) compounds[42–46] and 2.41–2.54 Å for other germyl compounds[47–51]}. Furthermore, the Mn–Ge distance in **6** is substantially shorter than in the previously reported $[(dmpe)_2Mn(=GePhR)]$ (**1a**: R = Ph, **2b**: R = H) derivatives which feature Mn–Ge distances of 2.2636(4) Å (**1a**) or 2.2462(6) Å (**2b**),[31] presumably due to increased π-backdonation in **6** (*vide infra*).

To the best of our knowledge, complex **6** is the first crystallographically characterized transition metal germylene complex with a terminal formate substituent. Notably, the formate substituent on Ge is κ^1-coordinated, in contrast to crystallographically characterized terminal formatostannylene complexes in which the formate substituent is κ^2-coordinated to tin.[52,53]

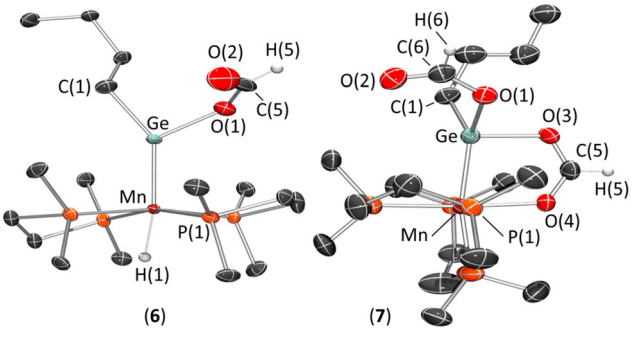

Fig. 1 X-ray crystal structures of (left) $[(dmpe)_2MnH\{=Ge^nBu(\kappa^1\text{-}O_2CH)\}]$ (**6**) and (right) $[(dmpe)_2Mn\{\kappa^2\text{-}Ge^nBu(\kappa^1\text{-}O_2CH)(OCHO)\}]$ (**7**). Ellipsoids are shown at 50% probability, and most hydrogen atoms were omitted for clarity (the hydride ligand in **6** was located from the difference map and refined isotropically). For complex **6**, one of the dmpe ligands and the $CH_2CH_2CH_3$ group are disordered over two positions, and only the dominant (81.9(16) and 84.7(7)%, respectively) components are shown.

In the absence of a second equivalent of CO_2, complex **6** decomposed at room temperature over several days (~30% conversion after 24 hours) to afford the previously reported[38] manganese(I) carbonyl hydride complex $[(dmpe)_2MnH(CO)]$ (**4**) as the major product; Scheme 4. However, in the presence of excess CO_2, **6** reacted with an additional equivalent of carbon dioxide to yield the κ^2-formatogermyl complex $[(dmpe)_2Mn\{\kappa^2\text{-}Ge^nBu(\kappa^1\text{-}O_2CH)(OCHO)\}]$ (**7**). This reaction proceeded to completion within 2 hours, presumably *via* a pathway analogous to that for conversion of germylene hydride complexes **1a–b** into κ^2-formatogermyl complexes **5a–b**.

Unlike the unstable κ^2-formatogermyl complexes **5a–b** (where R and R′ are hydrocarbyl groups), analytically pure **7** was isolated as dark red crystals in 63% yield and is stable in solution for days (although heating the reaction mixture at 80 °C resulted in conversion to **3** accompanied by unidentified by-products; potentially germoxane oligomers "OGe^{n}BuH" and/or their decomposition products). To the best of our knowledge, **7** is the first isolated example of a κ^2-formatogermyl transition metal complex (containing a 5-membered M–Ge–O–C(H)–O ring), although an unstable Os(III) κ^2-formatogermyl species has been characterized *in situ* by NMR spectroscopy (and osmium κ^2-carboxylatogermyl analogues were isolated).[54] Asymmetric O–C–O vibrations were located in the IR spectrum of complex **7** at 1577 and 1649 cm^{-1} for the bridging and terminal formate groups, respectively.

NMR spectra of **7** feature two sets of nearly overlapping environments from a pair of diastereomers in an approximate 1 : 2 ratio. Multiple ^{31}P NMR environments were observed for each diastereomer, indicative of disphenoidal dmpe coordination to manganese. EXSY NMR cross-peaks between PMe protons in the minor and major diastereomer indicate that the diastereomers slowly exchange, either by dissociation (from Mn) of one formate substituent on Ge and coordination of the other formate, or inversion of chirality at Mn *via* a 5-coordinate intermediate. For the two diastereomers, the terminal formate group gave rise to singlets in the ^{1}H and $^{13}C\{^1H\}$ NMR spectra at 8.78–8.79 and 164.5–164.9 ppm, respectively, similar to the singlets at 8.8–8.9 and 164–165 ppm from the terminal formate environment in **6** (and in **11**; *vide infra*). The second set of formate NMR environments in complex **7** (a singlet at 7.83–7.84 ppm in the ^{1}H NMR spectrum, and a doublet at 173.0–173.1 ppm in the $^{13}C\{^1H\}$ NMR spectrum with $^3J_{C,P}$ = 5–6 Hz) is consistent with a bridging formate group. For comparison, in **5a** the bridging formate ligand gave rise to a singlet in the ^{1}H NMR spectrum at 8.1 ppm and a doublet at 172.7 ppm in the $^{13}C\{^1H\}$ NMR spectrum with $^3J_{C,P}$ of 7 Hz.

X-ray quality crystals of κ^2-formatogermyl complex **7** were obtained from hexanes at −30 °C. The structure (Fig. 1; right) features a 5-membered Mn–Ge–O–C(H)–O ring, along with terminal *n*-butyl and formate substituents on the Ge atom. Given the reasonably high standard deviations involving certain bond metrics, DFT calculations (adf/ams, gas phase, all-electron, PBE, TZ2P, ZORA, D3-BJ; energy minima were located for both diastereomers) were also carried out (Table 1). The Mn–Ge distance of 2.341(2) Å in complex **7** (calcd 2.34 Å,

Table 1 Selected DFT-calculated and crystallographic bond distances in Å (and Mayer bond orders) involving the 5-membered metallacycles in κ^2-formatogermyl complexes [(dmpe)$_2$Mn{κ^2-GeRR′(OCHO)}] (**5a**: R = R′ = Ph, **5b**: R = R′ = Et, **7**: R = ^{n}Bu and R′ = κ^1-O$_2$CH) and κ^2-amidinylgermyl complexes [(dmpe)$_2$Mn{κ^2-GeRR′(N^{i}PrCHN^{i}Pr)}] (**9a**: R = R′ = Ph, **9b**: R = R′ = Et, **10**: R = ^{n}Bu and R′ = H, **11**: R = ^{n}Bu and R′ = κ^1-O$_2$CH). O$_{Ge}$, O$_{Mn}$, N$_{Ge}$, and N$_{Mn}$ are oxygen or nitrogen atoms bonded to Ge or Mn atoms in the 5-membered metallacycle. For complexes **7**, **10**, and **11**, DFT values for two diastereomers (arising from stereocenters on Mn and Ge) are included in the provided ranges. For complex **9a**, XRD values from two independent and essentially isostructural molecules in the unit cell are provided

	RR′		Mn–Ge	Mn–O$_{Mn}$	Ge–O$_{Ge}$	C–O$_{Ge}$	C–O$_{Mn}$
5a	Ph$_2$	DFT	2.39 (0.92)	2.20 (0.42)	2.03 (0.51)	1.28 (1.31)	1.25 (1.51)
5b	Et$_2$	DFT	2.40 (0.96)	2.20 (0.42)	2.04 (0.51)	1.28 (1.32)	1.25 (1.51)
7	^{n}Bu(κ^1-O$_2$CH)	DFT	2.34 (1.01–1.03)	2.11 (0.46–0.47)	2.02–2.03 (0.55)	1.28 (1.31–1.32)	1.26 (1.48)
		XRD	2.341(2)	2.117(7)	1.987(7)	1.27(1)	1.25(1)
	RR′		Mn–Ge	Mn–N$_{Mn}$	Ge–N$_{Ge}$	C–N$_{Ge}$	C–N$_{Mn}$
9a	Ph$_2$	DFT	2.43 (0.78)	2.15 (0.56)	1.97 (0.71)	1.34 (1.27)	1.31 (1.48)
		XRD	2.458(1)–2.461(1)	2.152(4)–2.179(8)	1.923(4)–1.946(5)	1.346(9)–1.363(7)	1.299(7)–1.319(8)
9b	Et$_2$	DFT	2.45 (0.78)	2.14 (0.60)	1.99 (0.65)	1.34 (1.28)	1.31 (1.48)
10	^{n}BuH	DFT	2.39–2.40 (0.85)	2.15–2.17 (0.55–0.57)	1.96 (0.73–0.74)	1.33–1.34 (1.27–1.28)	1.31 (1.48–1.49)
11	^{n}Bu(κ^1-O$_2$CH)	DFT	2.37–2.38 (0.90–0.91)	2.15–2.16 (0.57–0.59)	1.95 (0.75–0.77)	1.34 (1.25–1.26)	1.31 (1.48–1.49)
		XRD	2.378(1)	2.162(5)	1.919(5)	1.343(8)	1.293(7)

Mayer b.o. 1.01–1.03) is significantly longer than in germylene complex **6**, though on the shorter end of those for manganese(I) germyl complexes (2.29–2.54 Å).[55] The Mn–O distance of 2.117(7) Å in **7** (calcd 2.11 Å, Mayer b.o. 0.46–0.47) is longer than in formate complex **3** (2.086(1)–2.096(1) Å)[36] and other terminal manganese(I) formate complexes (1.94–2.10 Å).[55]

Within the bridging formate group in complex **7**, the C–O bond closest to Ge (C–O$_{Ge}$; 1.27(1) Å, calcd 1.28 Å, Mayer b.o. 1.31–1.32) is marginally longer than that close to Mn (C–O$_{Mn}$; 1.25(1) Å, calcd 1.26 Å, Mayer b.o. 1.48), while both are intermediate between a typical single and double C–O bond.[56] This suggests that **7** can be described using the two resonance structures in Fig. 2, with the former structure playing a slightly greater role (see SI for further discussion). Analogous canonical forms have been used to describe bonding in transition metal complexes featuring M–Ge–O–C(H)–N (M = Fe, W, Mo) or W–Ge–N–C(H)–S metallacycles.[25,27,28]

In order to probe how the substituents on Ge affect bonding in the κ^2-formatogermyl complexes, the metrics discussed above for complex **7** (featuring an *n*-butyl and a terminal formate substituent on germanium) were compared to calculated values for the GePh$_2$ and GeEt$_2$ derivatives **5a–b** (Tables 1 and S15). The substituents on germanium were found to have a limited impact on the C–O bonds in the bridging formate group or the Ge–O bond. However, both the Mn–Ge and Mn–O distances are slightly shorter (by 0.05–0.09 Å) in **7** relative to **5a–b**, with Mayer bond orders that are higher by 0.04–0.09.

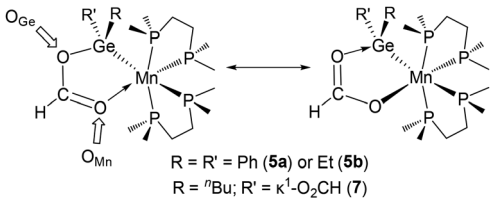

Fig. 2 Resonance structures for κ^2-formatogermyl complexes [(dmpe)$_2$Mn{κ^2-GeRR′(OCHO)}] (**5a**: R = R′ = Ph, **5b**: R = R′ = Et, **7**: R = ^{n}Bu and R′ = κ^1-O$_2$CH). Only one diastereomer is shown for complex **7**. The O$_{Ge}$ and O$_{Mn}$ environments discussed in the text and in Table 1 are indicated on the left structure.

Reactions of germylene hydride complexes with benzophenone

Similar to reactions of transition metal germylene complexes with carbon dioxide, reactions with ketones are fairly unexplored (*vide supra*). The bis(hydrocarbyl)germylene manganese(I) hydride complexes **1a–b** did not react with benzophenone, even at elevated temperature (60–85 °C). However, [(dmpe)$_2$MnH(=Ge^{n}BuH)] (**2a**), which features a terminal Ge–H bond, reacted with one equivalent of benzophenone at room temperature over 1 week (or overnight at 55 °C) to afford an alkoxygermylene complex, [(dmpe)$_2$MnH{=Ge^{n}Bu(OCHPh$_2$)}] (**8**); Scheme 5. This reaction may follow a pathway similar to that of **2a** with CO$_2$ to afford the formate-substituted germylene complex **6**. Complex **8** did not react with a second equivalent of benzophenone, even at elevated temperature, and is remarkably stable (relative to formatogermylene complex **6**) with only minor (<10%) decomposition overnight in solution at 100 °C.

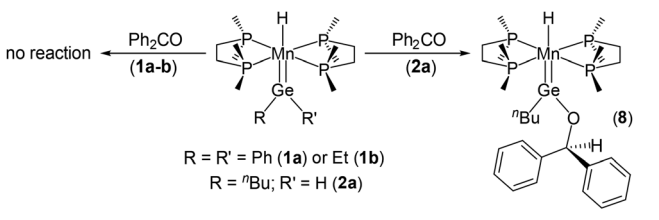

Scheme 5 Reactions of diorganylgermylene manganese(I) hydride complexes [(dmpe)$_2$MnH(=GeRR′)] (**1a**: R = R′ = Ph, **1b**: R = R′ = Et, **2a**: R = ^{n}Bu and R′ = H) with Ph$_2$CO.

Alkoxygermylene hydride complex **8** was isolated in 43% yield as very dark red X-ray quality crystals. Similar to other *trans*-diorganylgermylene manganese(I) hydride complexes (**1a–b**, **2a–b**, and **6**), complex **8** gave rise to a quintet in the ^{1}H NMR spectrum at −12.2 ppm ($^{2}J_{H,P}$ = 53 Hz) arising from the metal hydride, and a singlet in the ^{31}P{^{1}H} NMR spectrum at 78.9 ppm. The ^{1}H NMR spectrum also contains a reasonably high frequency singlet at 6.4 ppm due to the GeOC*H*Ph$_2$ environment. As expected for a germylene complex, the crystal structure of **8** (Fig. 3; left) displays a planar Ge environment (Σ(X–Ge–Y) = 359.7(1)°) and a short Mn–Ge distance of 2.2164 (7) Å, which is intermediate between that in formatogermylene complex **6** (2.201(1) Å) and previously reported[31] GePh$_2$ and GePhH derivatives **1a** and **2b** (2.2462(6)–2.2636(4) Å). Furthermore, an Mn–H stretch was located at 1705 cm^{-1} in the IR spectrum of complex **8** (*cf.* 1709 and 1685 cm^{-1} in **1a** and **1b**, respectively).

Reactions of germylene hydride complexes with C(N^{i}Pr)$_2$

Reactions of diorganylgermylene manganese(I) hydride complexes **1a–b** and **2a** with diisopropylcarbodiimide {C(N^{i}Pr)$_2$} afforded a family of metallacyclic κ^2-amidinylgermyl complexes [(dmpe)$_2$Mn{κ^2-GeRR′(N^{i}PrCHN^{i}Pr)}] (**9a**: R = R′ = Ph, **9b**: R = R′ = Et, **10**: R = ^{n}Bu and R′ = H), which were isolated in 15–67% yield with (for **9a–b**) analytical purity or (for **10**) > 95% purity as orange solids (Scheme 6). These reactions presumably proceed *via* a pathway analogous to that for the synthesis of κ^2-formatogermyl complexes **5a–b**. Furthermore, this reactivity is directly analogous to that of the silicon congeners, which resulted in κ^2-amidinylsilyl complexes [(dmpe)$_2$Mn{κ^2-SiRR′(N^{i}PrCHN^{i}Pr)}] (*vide supra*), and resembles the reactions of tungsten germylene hydride complexes with isocyanates or isothiocyanates to afford W–Ge–E–C(H)–N (E = O, S) metallacycles.[28,29]

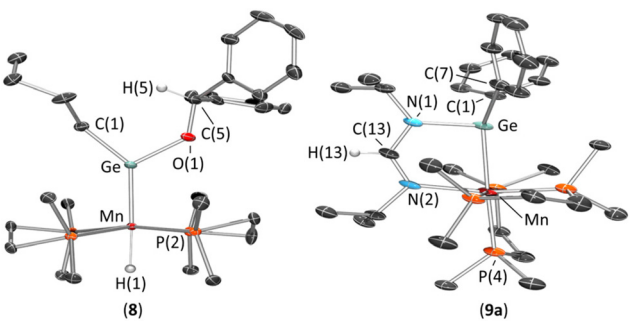

Fig. 3 X-ray crystal structures of (left) [(dmpe)$_2$MnH{=Ge^{n}Bu(OCHPh$_2$)}] (**8**) and (right) [(dmpe)$_2$Mn{κ^2-GePh$_2$(N^{i}PrCHN^{i}Pr)}] (**9a**). Ellipsoids are shown at 50% probability, and most hydrogen atoms are omitted for clarity (the hydride ligand in **8** was located from the difference map and refined isotropically). For complex **8**, the CH_2CH_3 group of the *n*-butyl substituent and a phenyl ring are disordered, and only the major components (53.6(5) and 54.5(8)%, respectively) are shown. The unit cell of complex **9a** contains two independent but essentially isostructural molecules, and only one is shown.

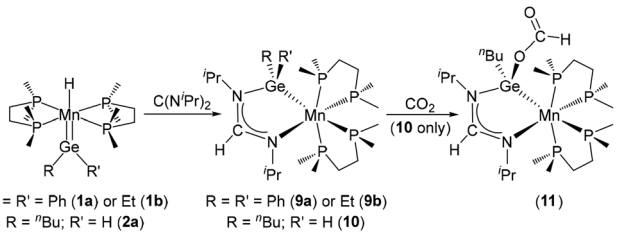

Scheme 6 Reactions of diorganylgermylene manganese(I) hydride complexes [(dmpe)$_2$MnH(=GeRR′)] (**1a**: R = R′ = Ph, **1b**: R = R′ = Et, **2a**: R = ^{n}Bu and R′ = H) with diisopropylcarbodiimide to afford κ^2-amidinylgermyl complexes [(dmpe)$_2$Mn{κ^2-GeRR′(N^{i}PrCHN^{i}Pr)}] (**9a**: R = R′ = Ph, **9b**: R = R′ = Et, **10**: R = ^{n}Bu and R′ = H), and the reaction of **10** with carbon dioxide to afford [(dmpe)$_2$Mn{κ^2-Ge^{n}Bu(κ^1-O$_2$CH)(N^{i}PrCHN^{i}Pr)}] (**11**). Only one diastereomer is shown for **10** and **11**.

NMR spectra of **9a–b** and **10** resemble those of the κ^2-formatogermyl complexes [(dmpe)$_2$Mn{κ^2-GeR$_2$(OCHO)}] (**5a**: R = Ph, **5b**: R = Et) and [(dmpe)$_2$Mn{κ^2-Ge^{n}Bu(κ^1-O$_2$CH)(OCHO)}] (**7**), as well as the previously reported κ^2-amidinylsilyl derivatives,[36] including high frequency signals in the ^{1}H (**9a**: 7.9 ppm, **9b**: 7.8 ppm, **10**: 7.6 ppm) and ^{13}C{^{1}H} (**9a**: 160.7 ppm, **9b**: 160.0 ppm, **10**: 159.6–159.7 ppm) NMR spectra arising from the central CH group of the amidinate moiety. In each case, four ^{31}P NMR environments were observed, indicative of disphenoidal dmpe coordination to manganese. Solutions containing the derivative with a terminal GeH substituent, **10**, gave rise to two sets of nearly identical NMR environments in a 1 : 0.75 ratio from the two diastereomers present in solution, with the Ge*H* ^{1}H NMR signals at 5.9–6.0 ppm (a broad peak assigned to the Ge–H stretch was also located in the IR spectrum of **10** at 1797 cm^{-1}). The formation of **10**, rather than the [(dmpe)$_2$MnH{=Ge^{n}Bu(κ^1-N^{i}PrCHN^{i}Pr)}] isomer, contrasts the reactivity of **2a** with CO_2 to form [(dmpe)$_2$MnH{=Ge^{n}Bu(κ^1-O$_2$CH)}] (**6**), and suggests a stronger preference for an amidinate group to bridge between Ge and Mn relative to a formate group.§

Maintaining a solution of [(dmpe)$_2$Mn{κ^2-GePh$_2$(N^{i}PrCHN^{i}Pr)}] (**9a**) in hexanes at −30 °C afforded X-ray quality crystals containing two independent but essentially isostructural molecules in the unit cell (Table 1). The structure of **9a** (Fig. 3; right) features a Mn–Ge–N–C(H)–N ring system analogous to the Mn–Ge–O–C(H)–O ring in **7** and the Mn–Si–N–C(H)–N ring in the κ^2-amidinylsilyl complex [(dmpe)$_2$Mn{κ^2-SiPhH(N^{i}PrCHN^{i}Pr)}].[36]

Consistent with bond metrics for κ^2-formatogermyl complexes (*vide supra*), the unsaturated bonds on either side of the ring carbon in **9a** are of slightly different lengths, with the one closer to the metal (C–N$_{Mn}$) lying between 1.299(7) and 1.319

§A DFT calculated energy minimum for the unobserved germylene-hydride isomer of **10**, [(dmpe)$_2$MnH{=Ge^{n}Bu(κ^1-N^{i}PrCHN^{i}Pr)}] (Fig. S171), is 51 kJ mol^{-1} *higher* in energy than the global minimum for **10** (a κ^2-amidinylgermyl complex). For comparison, the observed formatogermylene-hydride complex [(dmpe)$_2$MnH{=Ge^{n}Bu(κ^1-O$_2$CH)}] (**6**) is 22 kJ mol^{-1} *lower* in energy than the unobserved κ^2-formatogermyl isomer [(dmpe)$_2$Mn{κ^2-Ge^{n}BuH(OCHO)}] (Fig. S170).

(8) Å (calcd 1.31 Å, Mayer b.o. 1.48), and the one closer to germanium (C–N_{Ge}) ranging from 1.346(9) to 1.363(7) Å (calcd 1.34 Å, Mayer b.o. 1.27). Both are intermediate between the average single (1.40 ± 0.04 Å) and double (1.28 ± 0.02 Å) bond lengths in crystallographic-characterized acyclic hydrocarbyl-saturated amidines (RN=C(R)–NR_2).[55] The trend in relative C–N bond orders (C–N_{Mn} > C–N_{Ge}) is mirrored by QTAIM ellipticity at the bond critical points (0.25 > 0.19), and together indicates that the bonding environment can be described using resonance structures analogous to those discussed for κ^2-formatogermyl complexes **5a–b** and **7** (Fig. 2). It is also notable that the Mn–Ge distances in **9a** (2.461(1)–2.458(1) Å) are significantly longer than in κ^2-formatogermyl complex **7** (2.341(2) Å), falling at the high end of the range for manganese germyl complexes (*vide supra*).

The κ^2-amidinylgermyl complexes [(dmpe)$_2$Mn{κ^2-GeRR′(N^{i}PrCHN^{i}Pr)}] (**9a–b** and **10**), like their silicon analogues,[36] did not react with a second equivalent of C(N^{i}Pr)$_2$. Furthermore, **9a–b** (which lack a GeH substituent) did not react with carbon dioxide at ambient temperature. However, the derivative containing a terminal Ge–H bond ([(dmpe)$_2$Mn{κ^2-Ge^{n}BuH(N^{i}PrCHN^{i}Pr)}]; **10**) reacted within minutes with CO_2 to afford a new κ^2-amidinylgermyl complex with a terminal formate substituent on germanium: [(dmpe)$_2$Mn{κ^2-Ge^{n}Bu(κ^1-O$_2$CH)(N^{i}PrCHN^{i}Pr)}] (**11**; Scheme 6).

Analytically pure **11** was isolated in 67% yield from *in situ*-generated **10** by recrystallization from hexanes at −30 °C. However, it slowly decomposed in solution at room temperature to a variety of unidentified products (~25% conversion after 24 hours). The formation of complex **11** could proceed *via* isomerization of **10** to a germylene hydride isomer [(dmpe)$_2$MnH{=Ge^{n}Bu(κ^1-N^{i}PrCHN^{i}Pr)}] (the amidinate-substituted analogue of formate-substituted **6**), followed by reactivity analogous to reactions of **1a–b** with CO_2.

As with the GeH-containing precursor **10**, NMR spectra of [(dmpe)$_2$Mn{κ^2-Ge^{n}Bu(κ^1-O$_2$CH)(N^{i}PrCHN^{i}Pr)}] (**11**) include two sets of nearly-overlapping environments from a pair of diastereomers (in a 1 : 0.35 ratio), with N*CH*N environments in the ^{1}H and ^{13}C{^{1}H} NMR spectra at 7.77–7.83 and 160.0–160.2 ppm, respectively, along with multiple ^{31}P NMR environments. Additional high frequency peaks arising from the terminal formate substituent on Ge were observed at 8.86–8.87 (^{1}H NMR) and 163.7–164.1 (^{13}C{^{1}H} NMR) ppm. Two peaks were observed in the region of the IR spectrum associated with terminal formate groups (1637 and 1658 cm^{-1}), and were assigned as asymmetric OCO vibrations from the two diastereomers of **11** (DFT calculations on these diastereomers also provided substantially different ν(OCO)$_{asym(terminal)}$ values of 1646 and 1665 cm^{-1}).

An X-ray crystal structure of formate-substituted κ^2-amidinylgermyl complex [(dmpe)$_2$Mn{κ^2-Ge^{n}Bu(κ^1-O$_2$CH)(N^{i}PrCHN^{i}Pr)}] (**11**; Fig. 4 left; Table 1) confirmed that the amidinate and formate groups occupy bridging and terminal positions, respectively {and DFT calculations indicate that the isomer of **11** with the formate in a bridging position and a terminal amidinate group (Fig. S172) is 14 kJ mol^{-1} higher in energy than the global minimum for complex **11**}. Compound **11** is essentially isostructural to **9a**, with C–N_{Ge} and C–N_{Mn} distances of 1.343(8) and 1.293(7) Å, respectively (calcd 1.34 Å with Mayer b.o. 1.25–1.26, and 1.31 Å with Mayer b.o. 1.48–1.49, respectively) and a relatively planar environment about the Ge atom, not including the amidinate group (Σ(X–Ge–Y) = 356.3(2)°).

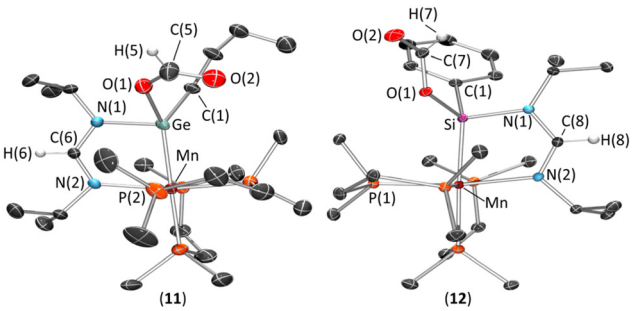

Fig. 4 X-ray crystal structures of (left) [(dmpe)$_2$Mn{κ^2-Ge^{n}Bu(κ^1-O$_2$CH)(N^{i}PrCHN^{i}Pr)}] (**11**) and (right) [(dmpe)$_2$Mn{κ^2-SiPh(κ^1-O$_2$CH)(N^{i}PrCHN^{i}Pr)}] (**12**). Ellipsoids are shown at 50% probability, and most hydrogen atoms are omitted for clarity.

As with κ^2-formatogermyl complexes discussed above, the substituents on Ge do not significantly affect C–N bonding within the metallacycle; for **9a–b**, **10**, and **11**, the corresponding C–N distances are calculated to be within 0.01 Å for each derivative (Table 1). Additionally, IR spectra of **9a–b**, **10**, and **11** feature asymmetric NCN stretches within a very narrow range (1589–1600 cm^{-1}). However, the Mn–Ge distances are more significantly influenced by the substitutents on Ge, with DFT-calculated distances increasing from 2.37–2.38 Å (Mayer b.o. 0.90–0.91, XRD: 2.378(1) Å) in [(dmpe)$_2$Mn{κ^2-Ge^{n}Bu(κ^1-O$_2$CH)(N^{i}PrCHN^{i}Pr)}] (**11**), to 2.39–2.40 Å (Mayer b.o. 0.85) in [(dmpe)$_2$Mn{κ^2-Ge^{n}BuH(N^{i}PrCHN^{i}Pr)}] (**10**), and 2.43–2.45 Å (Mayer b.o. of 0.78) in the diethyl and diphenyl derivatives **9a–b** (Table 1).

Intrigued by the reaction of **10** with CO_2, we tested analogous reactivity for the previously reported[36] κ^2-amidinylsilyl derivative [(dmpe)$_2$Mn{κ^2-SiPhH(N^{i}PrCHN^{i}Pr)}]. Indeed, upon exposure to CO_2 this complex underwent immediate and quantitative conversion to the formate-substituted κ^2-amidinylsilyl complex [(dmpe)$_2$Mn{κ^2-SiPh(κ^1-O$_2$CH)(N^{i}PrCHN^{i}Pr)}] (**12**; Scheme 7). The solid state structure (Fig. 4; right) and NMR spectra of complex **12** closely resemble those of the germa-

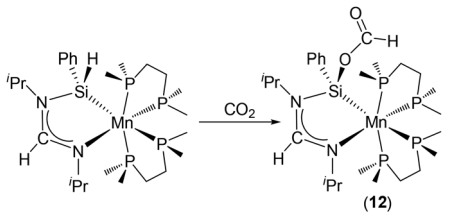

Scheme 7 Reaction of manganese κ^2-amidinylsilyl complex [(dmpe)$_2$Mn{κ^2-SiPhH(N^{i}PrCHN^{i}Pr)}] with carbon dioxide. Only one diasteromer is shown for each complex.

nium derivative **11**. Also, relative to the SiH-containing starting material, the ^{29}Si NMR signals for the two diastereomers of **12** are shifted to higher frequency (97.1–98.0 ppm, relative to 87.1 ppm), and the crystallographic Mn–Si distance of 2.3139 (9) Å is significantly shorter than that in [(dmpe)$_2$Mn{κ^2-SiPhH(N^{i}PrCHN^{i}Pr)}] (2.347(1)–2.358(1) Å).

Computational investigation of Mn=Ge bonding in germylene hydride complexes

DFT calculations (adf/ams, gas phase, all-electron, ZORA, D3-BJ) were employed to investigate the effect that installing formate or alkoxy substituents on the germylene ligand has on the strength and nature of Mn–Ge bonding in diorganylgermylene manganese(I) hydride complexes. Geometry optimization (TZ2P, PBE) of formatogermylene complex [(dmpe)$_2$MnH{=Ge^{n}Bu(κ^1-O$_2$CH)}] (**6**) and alkoxygermylene complex [(dmpe)$_2$MnH{=Ge^{n}Bu(OCHPh$_2$)}] (**8**) afforded structures with Mn–Ge distances (Table 2) accurate to within 0.01 Å of the crystallographically determined values. The Mn–Ge Mayer bond orders in complexes **6** and **8** (1.43 and 1.39, respectively) are similar to the values of 1.40–1.44 previously calculated for diorganylgermylene manganese(I) hydride complexes with hydrocarbyl and/or hydride substituents on Ge, [(dmpe)$_2$MnH(=GeRR′)] (**1a**: R = R′ = Ph, **1b**: R = R′ = Et, **2a**: R = ^{n}Bu and R′ = H, **2b**: R = Ph and R′ = H).[31]

The nature of Mn–Ge bonding in germylene complexes **6** and **8** was further investigated *via* fragment interaction calculations using the energy decomposition analysis (EDA)[57] method of Ziegler and Rauk (Table 2; PBE0, QZ4P, corrected for linear dependency of the wave function). This approach affords an overall interaction energy between a neutral (dmpe)$_2$MnH fragment and a neutral free germylene ligand, ΔE_{int}, which is divided into five components (ΔE_{elec}, ΔE_{Pauli}, ΔE_{orb}, ΔE_{disp}, and ΔE_{prep}) as discussed in the SI.[58,59]

Comparing the results of these calculations to those previously conducted[31] on [(dmpe)$_2$MnH(=GeEt$_2$)] (**1b**) and [(dmpe)$_2$MnH(=Ge^{n}BuH)] (**2a**) allows for trends to be elucidated upon changing one of the germylene substituents (alkyl, H, formate, or alkoxide) while keeping the other substituent as an alkyl group (Et or ^{n}Bu) (Table 2). The overall interaction energies (ΔE_{int}) for the Mn=Ge bonds become more negative when changing the GeR substituent in the order H (**2a**; −265 kJ mol^{-1}) < alkyl (**1b**; −267 kJ mol^{-1}) < alkoxide (**8**; −270 kJ mol^{-1}) < formate (**6**; −279 kJ mol^{-1}). In particular, the stronger bonding involving the Ge^{n}Bu(κ^1-O$_2$CH) ligand in **6** is driven largely by a stronger orbital interaction and reduced Pauli repulsion, partially offset by a diminished electrostatic contribution and a higher preparation energy.

The deformation density ($\Delta\rho$) associated with the orbital interaction component (ΔE_{orb}) from fragment interaction calculations on **6** and **8** was further divided using the Extended Transition State and Natural Orbitals for Chemical Valence (ETS-NOCV) method (Table 2 includes the energies for each component, along with literature data[31] for **1b** and **2a**). Deformation density isosurfaces and the main fragment orbital contributors are shown in Fig. 5.

Similar to previously reported ETS-NOCV calculations for **1a–b** and **2a–b** (for **1b** and **2a**, see Table 2),[31] the orbital component of the metal–germylene bond in **6** and **8** decomposes into three contributions; $\Delta\rho_\sigma$ involving σ donation from the HOMO of the ligand to the LUMO of the metal fragment, $\Delta\rho_{\pi(\perp)}$ involving π backdonation from a Mn d orbital (the HOMO of the metal-based fragment) to the LUMO of the ligand fragment, and a weaker $\Delta\rho_{\pi(\parallel)}$ interaction corresponding to π-backdonation within the plane of the germylene ligand. The acceptor orbital for the $\Delta\rho_{\pi(\perp)}$ interaction is π-antibonding with respect to the Ge–O bond, and is primarily composed of the vacant p orbital on germanium. By contrast, the acceptor orbital for the $\Delta\rho_{\pi(\parallel)}$ interaction is σ-antibonding with respect to the Ge–O bond, reminiscent of the acceptor orbitals for phosphine[60] and chalcogenoether[61,62] ligands, which are σ-antibonding with respect to the E–R (E = P, S, Se) bonds.

Table 2 Selected computational data, including fragment interaction {(dmpe)$_2$MnH + GeRR′} calculation data, pertaining to the Mn=Ge bonds in [(dmpe)$_2$MnH{=Ge^{n}Bu(κ^1-O$_2$CH)}] (**6**) and [(dmpe)$_2$MnH{=Ge^{n}Bu(OCHPh$_2$)}] (**8**), as well as previously reported data for [(dmpe)$_2$MnH(=GeEt$_2$)] (**1b**) and [(dmpe)$_2$MnH(=Ge^{n}BuH)] (**2a**).[31] The same computational method was used for all complexes, all energies are in kJ mol^{-1}, ΔE_{int} values are BSSE-corrected, and for ETS-NOCV data, values in parentheses are a percentages of ΔE_{orb}. HC = fragment Hirshfeld charge, [M] = (dmpe)$_2$MnH

		1b	**2a**	**6**	**8**
RR′		Et$_2$	^{n}BuH	^{n}Bu(κ^1-O$_2$CH)	^{n}Bu(OCHPh$_2$)
d(Mn–Ge)		2.25 Å	2.24 Å	2.20 Å	2.22 Å
Mayer b.o.		1.41	1.44	1.43	1.39
EDA	ΔE_{elec}	−490	−484	−444	−463
	ΔE_{orb}	−305	−317	−344	−313
	ΔE_{Pauli}	558	549	517	537
	ΔE_{Disp}	−40	−31	−42	−52
	ΔE_{prep}	8	17	32	20
	BSSE	1	1	2	2
	ΔE_{int}	−267	−265	−279	−270
HC	[M]	0.26	0.29	0.34	0.27
	GeRR′	−0.26	−0.29	−0.34	−0.27
ETS-NOCV	ΔE_σ	−134 (44%)	−135 (43%)	−120 (35%)	−124 (40%)
	$\Delta E_{\pi\perp}$	−117 (38%)	−127 (40%)	−135 (39%)	−113 (36%)
	$\Delta E_{\pi\parallel}$	−34 (11%)	−37 (12%)	−57 (16%)	−48 (15%)
	other	−20 (7%)	−17 (5%)	−32 (9%)	−28 (9%)

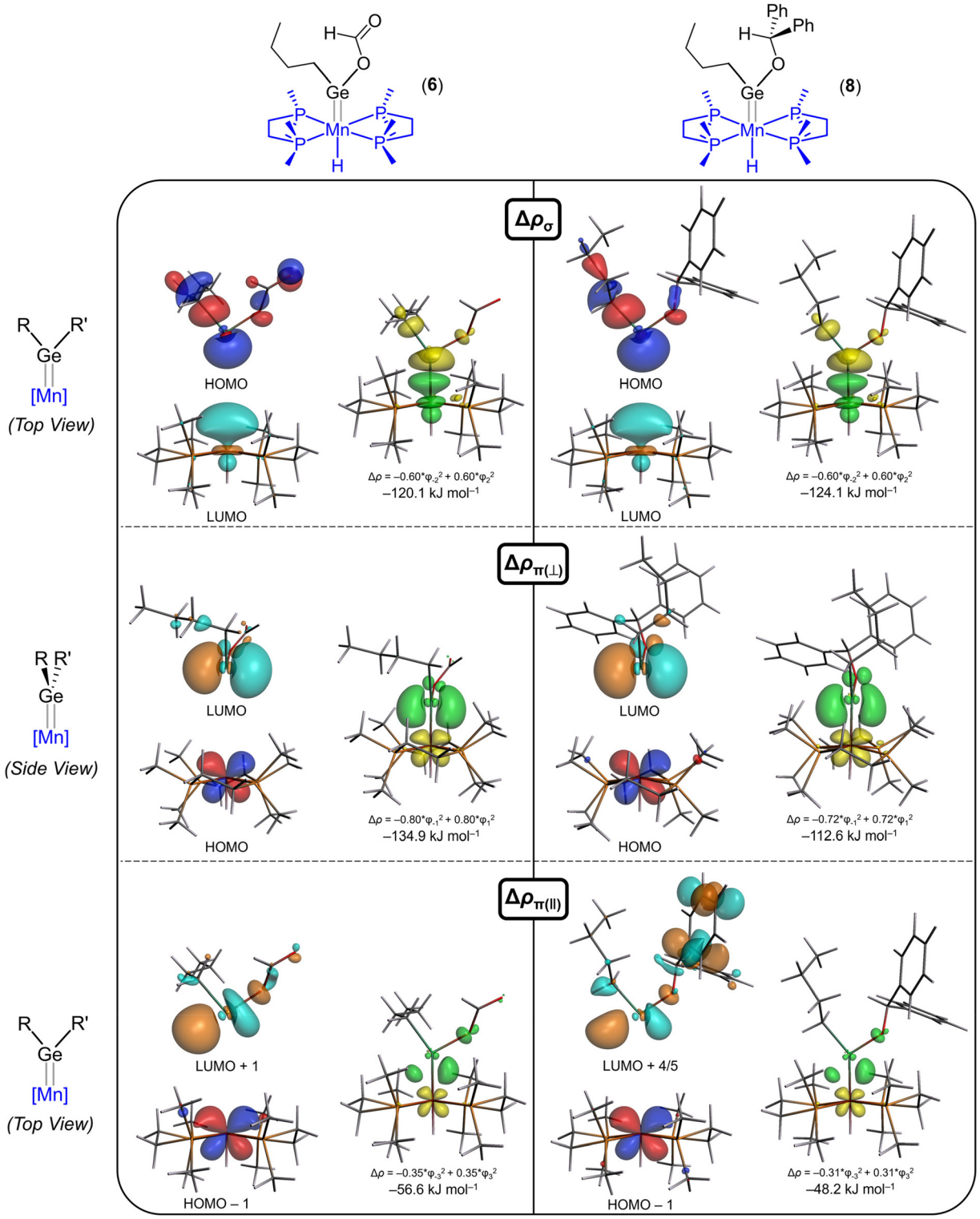

Fig. 5 Deformation density contributions and the main fragment orbital contributors to bonding between the $(dmpe)_2MnH$ and germylene fragments in $[(dmpe)_2MnH\{{=}Ge^nBu(\kappa^1\text{-}O_2CH)\}]$ (**6**; left) or $[(dmpe)_2MnH\{{=}Ge^nBu(OCHPh_2)\}]$ (**8**; right). Three major interactions were observed ($\Delta\rho_\sigma$, $\Delta\rho_{\pi(\perp)}$, and $\Delta\rho_{\pi(\parallel)}$). Deformation density isosurfaces (set to 0.003) are shown in green and yellow, corresponding to increased (green) and decreased (yellow) electron density relative to the non-interacting fragments. Orbital isosurfaces are set to 0.05. The germylene acceptor orbital for $\Delta\rho_{\pi(\parallel)}$ in complex **8** is a linear combination of the LUMO+4 and LUMO+5 (see Fig. S175). [In the ETS-NOCV calculation on complex **8**, the $\Delta\rho_{\pi(\parallel)}$ contribution lists two significant acceptor orbitals for the $Ge^nBu(OCHPh_2)$ fragment with SFO contributions of 0.010 (LUMO+4) and 0.013 (LUMO+5). Both of these orbitals are delocalized across the fragment. Linear combinations of these orbitals resulted in (i) an orbital which is σ-antibonding with respect to the Ge–O bond (included in Fig. 5) and can overlap with a donor orbital from the $(dmpe)_2MnH$ fragment, and (ii) an orbital associated with the π systems of the phenyl rings (see Fig. S175) which does not play a significant role in Mn═Ge bonding.]

For both the formatogermylene- and alkoxygermylene-complexes (**6** and **8**), the $\Delta\rho_{\sigma}$ and $\Delta\rho_{\pi(\parallel)}$ components are weaker and stronger, respectively, than those in **1b** and **2a**, and in the case of **6**, the $\Delta\rho_{\pi(\perp)}$ component is also more significant. Overall, the formatogermylene ligand in **6** is a better π-acceptor and a worse σ-donor than $GeEt_2$ or Ge^nBuH, highlighting the strong σ-withdrawing and weak π-donating abilities of the formate substituent. The more negative Hirshfeld charge on the germylene fragment in complex **6** (from the fragment interaction calculations; Table 2) relative to those in **1b**, **2a**, or **8** is also indicative of overall greater charge transfer from the $(dmpe)_2MnH$ fragment to the germylene ligand, consistent with increased π-backdonation and decreased σ-donation.

Summary and conclusions

This work describes reactions of the bis(hydrocarbyl)germylene manganese(I) hydride complexes $[(dmpe)_2MnH(=GeR_2)]$ (**1a**: R = Ph, **1b**: R = Et) with CO_2 to afford κ^2-formatogermyl intermediates $[(dmpe)_2Mn\{\kappa^2\text{-}GeR_2(OCHO)\}]$ (**5a**: R = Ph, **5b**: R = Et), which ultimately converted to $[(dmpe)_2Mn(\kappa^1\text{-}O_2CH)(CO)]$ (**3**) under an atmosphere of CO_2 (or decomposed to $[(dmpe)_2MnH(CO)]$ (**4**) in the absence of CO_2). By contrast, addition of CO_2 to $[(dmpe)_2MnH(=Ge^nBuH)]$ (**2a**), which contains a terminal GeH substituent, afforded the formatogermylene hydride complex $[(dmpe)_2MnH\{=Ge^nBu(\kappa^1\text{-}O_2CH)\}]$ (**6**), which converted to the κ^2-formatogermyl complex $[(dmpe)_2Mn\{\kappa^2\text{-}Ge^nBu(\kappa^1\text{-}O_2CH)(OCHO)\}]$ (**7**). Complexes **1a–b** did not react with Ph_2CO, whereas **2a** reacted to form the alkoxygermylene hydride complex $[(dmpe)_2MnH\{=Ge^nBu(OCHPh_2)\}]$ (**8**). Diorganylgermylene manganese(I) hydride complexes **1a–b** and **2a** reacted with diisopropylcarbodiimide to afford the κ^2-amidinylgermyl complexes $[(dmpe)_2Mn\{\kappa^2\text{-}GeRR'(N^iPrCHN^iPr)\}]$ (**9a**: R = R′ = Ph, **9b**: R = R′ = Et, **10**: R = ^{n}Bu and R′ = H). Compound **10** (which contains a GeH substituent) reacted with CO_2 to afford a κ^2-amidinylgermyl complex with a terminal formate substituent on Ge: $[(dmpe)_2Mn\{\kappa^2\text{-}Ge^nBu(\kappa^1\text{-}O_2CH)(N^iPrCHN^iPr)\}]$ (**11**). A silicon-containing analogue of **11** (compound **12**) was also synthesized. Density Functional Theory calculations were carried out to investigate the nature of Mn=Ge bonding in **6** and **8** *versus* **1b** and **2a**.

Prior to this work, only 2 examples of reactions between d-block germylene complexes and CO_2 had been described, and reactions with carbodiimides were unexplored. Key features of the work are: (a) the observation of κ^2-formatogermyl intermediates $[(dmpe)_2Mn\{\kappa^2\text{-}GeRR'(OCHO)\}]$ (**5a–b** and **7**) in reactions of **1a–b** and **2a** with CO_2; this contrasts the reactivity of silylene hydride analogues which rapidly eliminated siloxane byproducts to afford **3**, without observable intermediates. These reactivity differences may stem from the greater strength of Si–O *versus* Ge–O bonds. (b) Increasing κ^2-formatogermyl complex stability in the order GeRR′ = $GeEt_2$ (**5b**) < $GePh_2$ (**5a**) ≪ $Ge^nBu(\kappa^1\text{-}O_2CH)$ (**7**). (c) The reactivity of $[(dmpe)_2MnH(=Ge^nBuH)]$ (**2a**) with $C(N^iPr)_2$ to form the κ^2-amidinylgermyl complex $[(dmpe)_2Mn\{\kappa^2\text{-}Ge^nBuH(N^iPrCHN^iPr)\}]$ (**10**), rather than the $[(dmpe)_2MnH\{=Ge^nBu(\kappa^1\text{-}N^iPrCHN^iPr)\}]$ isomer; this contrasts the reactivity of **2a** with CO_2 to form $[(dmpe)_2MnH\{=Ge^nBu(\kappa^1\text{-}O_2CH)\}]$ (**6**), indicating a stronger preference for an amidinate *versus* a formate group to bridge between Ge and Mn (this is also highlighted in the structure of **11**, and for Si and Mn, in the structure of **12**). (d) The $Ge^nBu(\kappa^1\text{-}O_2CH)$ ligand in **6** was found to be a significantly worse σ-donor and better π-acceptor (within and perpendicular to the plane of the germylene ligand) than $GeEt_2$ or Ge^nBuH. It is also notable that compound **6** is the first crystallographically characterized transition metal germylene complex with a terminal formate substituent, and to the best of our knowledge, **7** is the first isolated example of a κ^2-formatogermyl transition metal complex.

Experimental

General methods

See SI.

Monitoring of reactions of $[(dmpe)_2MnH(=GeR_2)]$ (1a: R = Ph, 1b: R = Et) with CO_2 to form $[(dmpe)_2Mn(\kappa^1\text{-}O_2CH)(CO)]$ (3) *via* the intermediates $[(dmpe)_2Mn\{\kappa^2\text{-}GeR_2(OCHO)\}]$ (5a: R = Ph, 5b: R = Et). (a) Approx. 10 mg of $[(dmpe)_2MnH(=GeR_2)]$ (**1a**: R = Ph, **1b**: R = Et) was dissolved in approx. 0.6 mL of C_6D_6, and the solution placed in a J-young NMR tube. The mixture was freeze/pump/thawed three times, and placed under 1 atm of CO_2 at 0 °C, sealed, and warmed to room temperature. The reaction mixture turned from bronze to bright red within 1 hour, and was monitored over time *in situ* by NMR spectroscopy. Complete conversion to $[(dmpe)_2Mn(\kappa^1\text{-}O_2CH)(CO)]$ (**3**) occurred within two days, at which time the solution had turned light yellow with white precipitate. (b) 16 mg (0.03 mmol) of $[(dmpe)_2MnH(=GePh_2)]$ (**1a**) was dissolved in approx. 0.6 mL of d_8-toluene, and the solution placed in a J-young NMR tube. The mixture was cooled to 0 °C and degassed under dynamic vacuum for 1 minute, after which it was placed under 1 atm of CO_2 at 0 °C, sealed, and warmed to room temperature. After 30 minutes at room temperature, the resulting red solution was cooled to −32 °C, and analyzed by NMR spectroscopy at that temperature to limit decomposition of the intermediate $[(dmpe)_2Mn\{\kappa^2\text{-}GePh_2(OCHO)\}]$ (**5a**) for *in situ* NMR analysis. Selected NMR data for the intermediate $[(dmpe)_2Mn\{\kappa^2\text{-}GePh_2(OCHO)\}]$ (**5a**) are as follows. **5a: ^{1}H NMR (d_8-toluene, 500 MHz, 298 K):** δ 8.05 (s, 1H, OC$\underline{H}$O), 7.99, 7.79 (2 × d, 2H, $^3J_{H,H}$ 7.2 Hz, *o*-Ph), 1.42, 0.83 (2 × d, 3H, $^2J_{H,P}$ 5.8 Hz, PC$\underline{H}_3$), 1.19 (d, 3H, $^2J_{H,P}$ 6.3 Hz, PC$\underline{H}_3$), 1.14 (m, 6H, PC$\underline{H}_3$), 1.06 (d, 6H, $^2J_{H,P}$ 6.1 Hz, PC$\underline{H}_3$), 0.61 (d, 3H, $^2J_{H,P}$ 5.5 Hz, PC$\underline{H}_3$). **^{1}H NMR (d_8-toluene, 500 MHz, 241 K):** δ 8.08 (s, 1H, OC$\underline{H}$O), 8.09 (d, 2H, $^3J_{H,H}$ 6.6 Hz, *o*-Ph), 7.87 (d, 2H, $^3J_{H,H}$ 7.0 Hz, *o*-Ph), 7.26 (t, 2H, $^3J_{H,H}$ 7.0 Hz, *m*-Ph), 7.22 (t, 2H, $^3J_{H,H}$ 7.2 Hz, *m*-Ph), 7.08 (t, $^3J_{H,H}$ 7.2 Hz, *p*-Ph),¶ 7.04 (t, $^3J_{H,H}$ 6.9 Hz, *p*-Ph),¶ 1.80, 1.55, 1.14, 0.55 (4 × m, PC$\underline{H}_2$),¶ 1.43 (d, 3H, $^2J_{H,P}$

¶This NMR environment was determined using TOCSY NMR spectroscopy or 2D NMR spectroscopy, so no integration is provided.

4.6 Hz, PC$\underline{H}_3$), 1.21 (d, 3H, $^2J_{H,P}$ 5.3 Hz, PC$\underline{H}_3$), 1.09 (m, 9H, PC$\underline{H}_3$), 1.04 (d, 3H, $^2J_{H,P}$ 5.9 Hz, PC$\underline{H}_3$), 0.86 (d, 3H, $^2J_{H,P}$ 5.2 Hz, PC$\underline{H}_3$), 0.58 (d, 3H, $^2J_{H,P}$ 4.4 Hz, PC$\underline{H}_3$). **^{13}C{^{1}H} NMR (d_8-toluene, 126 MHz, 241 K)**: δ 172.70 (d, $^3J_{C,P}$ 7.1 Hz, O$\underline{C}$HO), 160.98, 160.47 (2 × s, *i*-Ph), 132.36, 132.12 (2 × s, *o*-Ph), 126.31, 125.99 (2 × s, *m*-Ph), 37.09 (d, $J_{C,P}$ 13.6 Hz, P$\underline{C}$H$_3$), 35.18 (app. t, $J_{C,P}$ 21.8 Hz, P$\underline{C}$H$_2$), 34.53 (m, P$\underline{C}$H$_2$), 31.98 (m, P$\underline{C}$H$_2$), 24.10 (d, $J_{C,P}$ 13.0 Hz, P$\underline{C}$H$_3$), 23.71, 14.07 (2 × s, P$\underline{C}$H$_3$), 23.24 (d, $J_{C,P}$ 14.4 Hz, P$\underline{C}$H$_3$), 20.59 (P$\underline{C}$H$_3$),¶ 17.09 (d, $J_{C,P}$ 8.5 Hz, P$\underline{C}$H$_3$), 16.62 (d, $J_{C,P}$ 10.3 Hz, P$\underline{C}$H$_3$). **^{31}P{^{1}H} NMR (d_8-toluene, 202 MHz, 298 K)**: δ 82.89, 80.52, 72.66, 64.65 (4 × s, 1P). **^{31}P{^{1}H} NMR (d_8-toluene, 202 MHz, 241 K)**: δ 83.19, 80.54 (2 × s, 1P), 73.27 (app. q, $J_{P,P}$ 31.8 Hz, 1P), 64.86 (app. t, $J_{P,P}$ 31.5 Hz, 1P). Selected NMR data for the intermediate [(dmpe)$_2$Mn{κ^2-GeEt$_2$(OCHO)}] (**5b**) are: **^{1}H NMR (C_6D_6, 500 MHz, 298 K)**: δ 7.83 (s, 1H, OC$\underline{H}$O). **^{31}P{^{1}H} NMR (C_6D_6, 202 MHz, 298 K)**: δ 82.93, 78.11, 75.75, 67.87 (4 × s, 1P).

Monitoring of the reaction of [(dmpe)$_2$MnH(=GePh$_2$)] (1a) with CO_2 to form [(dmpe)$_2$MnH(CO)] (4) *via* the intermediate [(dmpe)$_2$Mn{κ^2-GePh$_2$(OCHO)}] (5a). 15.9 mg (0.03 mmol) of [(dmpe)$_2$MnH(=GePh$_2$)] (**1a**) was dissolved in ~0.6 mL of C_6D_6. The dark bronze reaction mixture was freeze/pump/thawed three times, and placed under 1 atm of CO_2 at 0 °C, sealed, and warmed to room temperature. After shaking, the mixture was allowed to sit at room temperature for 30 minutes to afford a royal red solution, and the solvent (and remaining CO_2) was removed *in vacuo*. The resulting red solid was dissolved in ~0.6 mL of C_6D_6, and the reaction mixture was monitored *in situ* by NMR spectroscopy after various time intervals. After 20 minutes, the reaction mixture contained **1a**, **3**, **4**, and **5a** in an approximate 1 : 0.3 : 0.3 : 3.5 ratio. After allowing to sit for 20 hours, the ratio became 1 : 0.5 : 6.3 : 0.3 (with minor decomposition to free dmpe and unidentified impurities also apparent).

Monitoring of the reaction of [(dmpe)$_2$MnH(=Ge^{n}BuH)] (2a) with excess CO_2 to sequentially form [(dmpe)$_2$MnH{=Ge^{n}Bu(κ^1-O$_2$CH)}] (6), [(dmpe)$_2$Mn{κ^2-Ge^{n}Bu(κ^1-O$_2$CH)(OCHO)}] (7), and [(dmpe)$_2$Mn(κ^1-O$_2$CH)(CO)] (3). Approx. 10 mg of [(dmpe)$_2$MnH(=Ge^{n}BuH)] (**2a**) was dissolved in approx. 0.6 mL of C_6D_6, and the solution placed in a J-young NMR tube. The mixture was freeze/pump/thawed three times, and placed under 1 atm of CO_2 at 0 °C, sealed, and warmed to room temperature. The reaction mixture turned from bronze to bright red within 1 hour, and was monitored over time *in situ* by NMR spectroscopy. After sitting for 2 days at room temperature (with periodic monitoring by NMR spectroscopy), the solution was heated at 80 °C and continued to be monitored periodically by NMR spectroscopy. Selected NMR data for [(dmpe)$_2$MnH{=Ge^{n}Bu(κ^1-O$_2$CH)}] (**6**) are as follows. **^{1}H NMR (C_6D_6, 500 MHz, 298 K)**: δ 8.75 (s, 1H, OC$\underline{H}$O), 1.73, 1.56 (2 × br. s, 4H, PC$\underline{H}_2$), 1.52, 1.12 (2 × s, 12H, PC$\underline{H}_3$), −11.76 (quin., 1H, $^2J_{H,P}$ 53.1 Hz, Mn$\underline{H}$). **^{13}C{^{1}H} NMR (C_6D_6, 151 MHz, 298 K)**: δ 165.21 (s, O$\underline{C}$HO), 34.16 (m, P$\underline{C}$H$_2$), 28.86, 27.81 (2 × s, P$\underline{C}$H$_3$). **^{31}P{^{1}H} NMR (C_6D_6, 243 MHz, 298 K)**: δ 77.66 (s).

Monitoring of the reaction of [(dmpe)$_2$MnH(=Ge^{n}BuH)] (2a) with limiting CO_2 to sequentially form [(dmpe)$_2$MnH{=Ge^{n}Bu(κ^1-O$_2$CH)}] (6) and [(dmpe)$_2$MnH(CO)] (4). 11.9 mg (0.02 mmol) of [(dmpe)$_2$MnH(=Ge^{n}BuH)] (**2a**) was dissolved in 0.58 mL of C_6D_6 and placed in a J-young NMR tube. The mixture was freeze/pump/thawed three times, and the headspace (1.72 mL) placed under 31.7 kPa of CO_2 (0.02 mmol) at 298 K and sealed. The reaction mixture was monitored *in situ* periodically by NMR spectroscopy.

X-ray crystal structure of [(dmpe)$_2$MnH{=Ge^{n}Bu(κ^1-O$_2$CH)}] (6). 15.0 mg (0.03 mmol) of [(dmpe)$_2$MnH(=Ge^{n}BuH)] (**2a**) was dissolved in 0.57 mL of C_6D_6 and placed in a J-young NMR tube. The mixture was freeze/pump/thawed three times, and the headspace (1.73 mL) placed under 39.7 kPa of CO_2 (0.03 mmol) at 298 K and sealed. The reaction was allowed to sit for 10 minutes, after which the solvent was removed *in vacuo*. X-ray quality crystals were obtained by recrystallization from a concentrated solution in hexamethyldisiloxane at −30 °C.

[(dmpe)$_2$Mn{κ^2-Ge^{n}Bu(κ^1-O$_2$CH)(OCHO)}] (7). 62.8 mg (0.13 mmol) of [(dmpe)$_2$MnH(=Ge^{n}BuH)] (**2a**) was dissolved in 5 mL of benzene and the solution placed in a 50 mL bomb. The mixture was freeze/pump/thawed three times, and placed under 1 atm of CO_2 at 0 °C, sealed, and warmed to room temperature. Stirring for 3 hours at room temperature resulted in a bright orange solution. The solvent was removed *in vacuo*, and the resulting red oil was dissolved in 2 mL of hexanes. This solution was allowed to sit at −30 °C to afford 35.7 mg (0.06 mmol) of [(dmpe)$_2$Mn{κ^2-Ge^{n}Bu(κ^1-O$_2$CH)(OCHO)}] (**7**) as dark red X-ray quality crystals (upon crushing, the solid became a bright red powder). Concentrating the mother liquor and allowing it to sit again at −30 °C afforded an additional 11.1 mg (0.02 mmol) of complex **7** (total yield 63%). IR (Nujol mull): $\nu(OCO)_{asym(terminal)}$ 1649 cm^{-1} (calcd 1639 and 1688 cm^{-1} for the lower and higher energy diastereomers, respectively), $\nu(OCO)_{asym(bridging)}$ 1577 cm^{-1} (calcd 1561 and 1557 cm^{-1} for the lower and higher energy diastereomers, respectively). Vis: λ_{max} 476 nm. Dominant diastereomer NMR data are as follows. **^{1}H NMR (C_6D_6, 600 MHz, 298 K)**: δ 8.78 (s, 1H, OC$\underline{H}$O terminal), 7.84 (s, 1H, OC$\underline{H}$O bridging), 2.24, 2.11 (2 × m, 1H, CH$_2$C$\underline{H}_2$CH$_2$CH$_3$), 2.12, 1.47 (2 × m, 1H, C$\underline{H}_2$CH$_2$CH$_2$CH$_3$), 1.94, 0.53 (2 × m, 1H, PC$\underline{H}_2$), 1.67 (m, 2H, PC$\underline{H}_2$), 1.61 (m, 2H, CH$_2$CH$_2$C$\underline{H}_2$CH$_3$), 1.57 (d, 3H, $^2J_{H,P}$ 6.5 Hz, PC$\underline{H}_3$), 1.52 (d, 3H, $^2J_{H,P}$ 5.2 Hz, PC$\underline{H}_3$), 1.48 (d, 3H, $^2J_{H,P}$ 5.8 Hz, PC$\underline{H}_3$), 1.15, 0.82 (2 × d, 3H, $^2J_{H,P}$ 5.3 Hz, PC$\underline{H}_3$), 1.14 (d, 3H, $^2J_{H,P}$ 6.0 Hz, PC$\underline{H}_3$), 1.09 (d, 3H, $^2J_{H,P}$ 4.7 Hz, PC$\underline{H}_3$), 1.06 (t, 3H, $^3J_{H,H}$ 7.3 Hz, CH$_2$CH$_2$CH$_2$C$\underline{H}_3$), 0.50 (s, 3H, PC$\underline{H}_3$). **^{13}C{^{1}H} NMR (C_6D_6, 151 MHz, 298 K)**: δ 173.12 (d, $^3J_{C,P}$ 5.1 Hz, O$\underline{C}$HO bridging), 164.92 (s, O$\underline{C}$HO terminal), 36.89 (s, $\underline{C}$H$_2$CH$_2$CH$_2$CH$_3$), 34.63, 34.19, 32.05 (3 × m, P$\underline{C}$H$_2$), 31.60 (d of m, $J_{C,P}$ 17.6 Hz, P$\underline{C}$H$_3$), 27.80 (s, CH$_2$$\underline{C}H_2CH_2CH_3$), 27.05 (s, CH$_2CH_2$$\underline{C}H_2CH_3$), 24.12, 22.67, 16.52 (3 × m, P$\underline{C}$H$_3$), 17.78 (d, $J_{C,P}$ 12.5 Hz, P$\underline{C}$H$_3$), 15.81 (d, $J_{C,P}$ 9.1 Hz, P$\underline{C}$H$_3$), 14.28 (s, CH$_2$CH$_2$CH$_2$$\underline{C}H_3$). **^{31}P{^{1}H} NMR ($C_6D_6$, 243 MHz, 298 K)**: δ 80.52 (s, 2P), 71.48, 65.54 (2 × s, 1P). Minor diastereomer NMR data are as follows. **^{1}H NMR (C_6D_6, 600 MHz, 298 K)**: δ 8.79 (s, 1H, OC$\underline{H}$O terminal), 7.83 (s, 1H, OC$\underline{H}$O bridging), 2.24, 2.13 (2 × m, 1H, CH$_2$C$\underline{H}_2$CH$_2$CH$_3$), 2.23, 1.61 (2 × m, 1H,

CH_2CH$_2$CH$_2$CH$_3$), 1.61 (m, 2H, CH$_2$CH$_2$CH_2CH$_3$), 1.56 (d, 3H, $^2J_{H,P}$ 5.3 Hz, PCH_3), 1.34 (d, 3H, $^2J_{H,P}$ 5.5 Hz, PCH_3), 1.25 (d, 3H, $^2J_{H,P}$ 5.4 Hz, PCH_3), 1.17 (d, 3H, $^2J_{H,P}$ 6.5 Hz, PCH_3), 1.11 (d, 3H, $^2J_{H,P}$ 6.4 Hz, PCH_3), 1.07 (m, 6H, PCH_3), 1.06 (t, 3H, $^3J_{H,H}$ 7.3 Hz, CH$_2$CH$_2$CH$_2$CH_3), 0.50 (s, 3H, PCH_3). **^{13}C{^{1}H} NMR (C$_6$D$_6$, 151 MHz, 298 K):** δ 173.00 (d, $^3J_{C,P}$ 6.4 Hz, OCHO bridging), 164.54 (s, OCHO terminal), 36.10 (s, CH$_2$CH$_2$CH$_2$CH$_3$), 34.89, 33.52, 32.68 (3 × m, PCH$_2$), 34.26, 23.76, 22.67 (3 × m, PCH$_3$), 32.31 (d, $J_{C,P}$ 17.9 Hz, PCH$_3$), 27.57 (s, CH$_2$CH$_2$CH$_2$CH$_3$), 27.09 (s, CH$_2$CH$_2$CH$_2$CH$_3$), 22.06 (d, $J_{C,P}$ 22.2 Hz, PCH$_3$), 19.70 (d, $J_{C,P}$ 12.1 Hz, PCH$_3$), 15.31 (d of d, $J_{C,P}$ 11.8 and 3.3 Hz, PCH$_3$), 14.26 (s, CH$_2$CH$_2$CH$_2$CH$_3$). **^{31}P{^{1}H} NMR (C$_6$D$_6$, 243 MHz, 298 K):** δ 81.81, 78.99, 75.24, 63.29 (4 × s, 1P). Anal. found (calcd): C, 37.24 (37.60); H, 7.71 (7.54); N, 4.89 (4.57).

[(dmpe)$_2$MnH{=Ge^{n}Bu(OCHPh$_2$)}] (8). 43.1 mg (0.09 mmol) of [(dmpe)$_2$MnH(=Ge^{n}BuH)] (**2a**) and 18.5 mg (0.10 mmol) of benzophenone were dissolved in 4 mL of benzene, and the reaction mixture was stirred overnight at 55 °C. The solvent was removed *in vacuo*, and the resulting very dark red solid was dissolved in ~1 mL of hexamethyldisiloxane. Solid residue was removed by centrifugation, and the mother liquor left to sit at −30 °C to afford 25.3 mg (0.04 mmol, 43%) of [(dmpe)$_2$MnH{=Ge^{n}Bu(OCHPh$_2$)}] (**8**) as X-ray quality dark red crystals. IR (Nujol mull): ν(Mn–H) 1705 cm^{-1} (calcd 1792 cm^{-1}). Vis: λ_{max} 416 nm. **^{1}H NMR (C$_6$D$_6$, 500 MHz, 298 K):** δ 7.60 (d, 4H, $^3J_{H,H}$ 7.1 Hz, *o*-Ph), 7.23 (t, 4H, $^3J_{H,H}$ 7.7 Hz, *m*-Ph), 7.07 (t, 2H, $^3J_{H,H}$ 6.8 Hz, *p*-Ph), 6.36 (s, 1H, OCHPh$_2$), 1.89, 1.63 (2 × m, 4H, PCH_2), 1.47 (m, 2H, CH$_2$CH_2CH$_2$CH$_3$), 1.44, 1.19 (2 × s, 12H, PCH_3), 1.36 (m, 2H, CH_2CH$_2$CH$_2$CH$_3$), 1.33 (sext., 2H, $^3J_{H,H}$ 7.2 Hz, CH$_2$CH$_2$CH_2CH$_3$), 0.87 (t, 3H, $^3J_{H,H}$ 7.3 Hz, CH$_2$CH$_2$CH$_2$CH_3), −12.22 (quin., $^2J_{H,P}$ 52.4 Hz, MnH). **^{13}C{^{1}H} NMR (C$_6$D$_6$, 126 MHz, 298 K):** δ 148.96 (s, *i*-Ph), 128.30 (s, *m*-Ph), 127.35 (s, *o*-Ph), 126.56 (s, *p*-Ph), 80.20 (s, OCHPh$_2$), 46.41 (s, CH$_2$CH$_2$CH$_2$CH$_3$), 34.37 (m, PCH$_2$), 29.60, 28.36 (2 × m, PCH$_3$), 27.44 (s, CH$_2$CH$_2$CH$_2$CH$_3$), 27.08 (s, CH$_2$CH$_2$CH$_2$CH$_3$), 13.98 (s, CH$_2$CH$_2$CH$_2$CH$_3$). **^{31}P{^{1}H} NMR (C$_6$D$_6$, 202 MHz, 298 K):** δ 78.92 (s). Anal. found (calcd): C, 52.10 (52.05); H, 8.16 (7.98).

[(dmpe)$_2$Mn{κ^2-GePh$_2$(N^{i}PrCHN^{i}Pr)}] (9a). 107.1 mg (0.18 mmol) of [(dmpe)$_2$MnH(=GePh$_2$)] (**1a**) was dissolved in 10 mL of benzene. 69 mg (0.55 mmol) of diisopropylcarbodiimide was added to the solution, and the reaction mixture stirred at room temperature for 2 days. The solvent was removed *in vacuo*, then an aliquot of the resulting red oil was analyzed by NMR spectroscopy to contain a significant amount of un-reacted **1a**. The oil was then dissolved in another 10 mL of benzene and an additional 70 mg (0.55 mmol) of diisopropylcarbodiimide was added. The solvent was again removed *in vacuo* and the resulting red oil was recrystallized from a concentrated solution in hexanes to afford 19.5 mg (0.03 mmol, 15%) of [(dmpe)$_2$Mn{κ^2-GePh$_2$(N^{i}PrCHN^{i}Pr)}] (**9a**) as X-ray quality orange crystals. IR (Nujol mull): ν(NCN)$_{asym(bridging)}$ 1597 cm^{-1} (calcd 1601 cm^{-1}). Vis: λ_{max} ~470 nm (shoulder). **^{1}H NMR (C$_6$D$_6$, 600 MHz, 298 K):** δ 7.93 (d, 2H, $^3J_{H,H}$ 6.6 Hz, *o*-Ph), 7.93 (s, NCHN), 7.80 (d, 2H, $^3J_{H,H}$ 6.7 Hz, *o*-Ph), 7.33, 7.28 (2 × t, 2H, $^3J_{H,H}$ 7.4 Hz, *m*-Ph), 7.25 (t, 1H, $^3J_{H,H}$ 7.3 Hz, *p*-Ph), 7.19 (t, 1H, $^3J_{H,H}$ 7.4 Hz, *p*-Ph), 3.91 (hept., 1H, $^3J_{H,H}$ 6.6 Hz, CHMe$_2$), 3.06 (hept., 1H, $^3J_{H,H}$ 6.5 Hz, CHMe$_2$), 2.40 (m, 1H, PCH_2), 1.91, 1.60 (2 × m, 2H, PCH_2), 1.67 (d, 3H, $^2J_{H,P}$ 5.6 Hz, PCH_3), 1.42, 1.10, 0.74 (3 × d, 3H, $^2J_{H,P}$ 4.3 Hz, PCH_3), 1.40 (d, 3H, $^2J_{H,P}$ 4.4 Hz, PCH_3), 1.39 (d, 3H, $^2J_{H,P}$ 6.2 Hz, PCH_3), 1.31 (m, 3H, PCH_2), 1.27, 1.03 (2 × d, 3H, $^3J_{H,H}$ 6.8 Hz, CH(CH_3)$_2$), 1.19 (d, 3H, $^2J_{H,P}$ 3.2 Hz, PCH_3), 0.93, 0.68 (2 × d, 3H, $^3J_{H,H}$ 6.5 Hz, CH(CH_3)$_2$), 0.89 (d, 3H, $^2J_{H,P}$ 5.7 Hz, PCH_3). **^{13}C{^{1}H} NMR (C$_6$D$_6$, 151 MHz, 298 K):** δ 160.70 (s, NCHN), 158.94 (s, *i*-Ph), 154.99 (m, *i*-Ph), 138.08, 136.62 (2 × s, *o*-Ph), 127.09, 126.87 (2 × s, *m*-Ph), 126.80, 126.13 (2 × s, *p*-Ph), 59.02 (d, $J_{C,P}$ 8.3 Hz, CHMe$_2$), 48.34 (s, CHMe$_2$), 36.37, 35.59, 32.71 (3 × m, PCH$_2$), 35.44, 22.36 (2 × m, PCH$_3$), 27.22 (app. t, $J_{C,P}$ 8.4 Hz, PCH$_3$), 26.19, 25.80, 25.35, 24.72 (4 × s, CH(CH$_3$)$_2$), 25.53 (d of d, $J_{C,P}$ 18.0 and 3.4 Hz, PCH$_3$), 24.63, 24.32 (2 × s, PCH$_3$), 23.08 (d, $J_{C,P}$ 17.5 Hz, PCH$_3$), 18.45 (d, $J_{C,P}$ 5.9 Hz, PCH$_3$). **^{31}P{^{1}H} NMR (C$_6$D$_6$, 243 MHz, 298 K):** δ 79.79, 73.93, 65.91, 61.36 (4 × s, 1P). Anal. found (calcd): C, 52.56 (52.50); H, 8.10 (8.10); N, 4.31 (3.95).

[(dmpe)$_2$Mn{κ^2-GeEt$_2$(N^{i}PrCHN^{i}Pr)}] (9b). 108.4 mg (0.22 mmol) of [(dmpe)$_2$MnH(=GeEt$_2$)] (**1b**) was dissolved in 10 mL of benzene. 84.3 mg (0.67 mmol) of diisopropylcarbodiimide was added, and the reaction mixture was stirred at room temperature overnight. The solvent was then removed *in vacuo* to afford an orange solid, which was dissolved in hexamethyldisiloxane and let sit at −30 °C to afford 61.8 mg (0.10 mmol) of [(dmpe)$_2$Mn{κ^2-GeEt$_2$(N^{i}PrCHN^{i}Pr)}] (**9b**) as an orange solid. Concentrating the mother liquor and letting it sit again at −30 °C afforded an additional 29.3 mg (0.05 mmol) of **9b**, for a total yield of 67%. IR (Nujol mull): ν(NCN)$_{asym(bridging)}$ 1600 cm^{-1} (calcd 1608 cm^{-1}). Vis: λ_{max} 464 nm. **^{1}H NMR (C$_6$D$_6$, 500 MHz, 298 K):** δ 7.70 (t, 1H, $^4J_{H,P}$ 2.0 Hz, NCHN), 3.88, 3.06 (2 × hept., 1H, $^3J_{H,H}$ 6.7 Hz, CHMe$_2$), 1.58–1.96 (m, 5H, PCH_2), 1.56 (m, 6H, CH$_2$CH$_3$), 1.53, 1.26 (2 × m, 2H, CH$_2$CH$_3$), 1.48 (d, 3H, $^2J_{H,P}$ 5.8 Hz, PCH_3), 1.38 (d, 3H, $^2J_{H,P}$ 5.3 Hz, PCH_3), 1.35 (d, 3H, $^2J_{H,P}$ 6.0 Hz, PCH_3), 1.34 (d, 3H, $^2J_{H,P}$ 4.8 Hz, PCH_3), 1.26 (m, 2H, PCH_2), 1.24 (d, 3H, $^2J_{H,P}$ 4.3 Hz, PCH_3), 1.19 (d, 3H, $^2J_{H,P}$ 3.1 Hz, PCH_3), 1.16, 0.96 (2 × d, 3H, $^3J_{H,H}$ 6.8 Hz, CH(CH_3)$_2$), 1.14 (d, 3H, $^3J_{H,H}$ 6.7 Hz, CH(CH_3)$_2$), 1.07 (d, 3H, $^2J_{H,P}$ 5.0 Hz, PCH_3), 0.98 (m, 1H, PCH_2), 0.89 (d, 3H, $^3J_{H,H}$ 6.6 Hz, CH(CH_3)$_2$), 0.84 (d, 3H, $^2J_{H,P}$ 4.5 Hz, PCH_3). **^{13}C{^{1}H} NMR (C$_6$D$_6$, 126 MHz, 298 K):** δ 160.04 (s, NCHN), 58.76 (d, $J_{C,P}$ 9.6 Hz, CHMe$_2$), 48.14 (s, CHMe$_2$), 36.78 (t of m, $J_{C,P}$ 21.8 Hz, PCH$_2$), 36.09 (t of t, $J_{C,P}$ 18.5 and 2.8 Hz, PCH$_2$), 35.04 (d of d, $J_{C,P}$ 23.3 and 16.7 Hz, PCH$_2$), 34.14, 26.69, 24.83, 24.09, 19.76 (5 × m, PCH$_3$), 32.29 (d of d, $J_{C,P}$ 21.7 and 16.4 Hz, PCH$_2$), 26.32, 25.61, 25.34, 24.48 (4 × s, CH(CH$_3$)$_2$), 25.98 (d of d, $J_{C,P}$ 17.4 and 3.8 Hz, PCH$_3$), 25.23 (d, $J_{C,P}$ 15.4 Hz, PCH$_3$), 18.37 (m, CH$_2$CH$_3$), 17.54 (d, $J_{C,P}$ 8.0 Hz, PCH$_3$), 16.83 (app. q, $J_{C,P}$ 4.9 Hz, CH$_2$CH$_3$), 12.24, 12.07 (2 × s, CH$_2$CH$_3$). **^{31}P{^{1}H} NMR (C$_6$D$_6$, 202 MHz, 298 K):** δ 76.05, 72.07, 69.92, 58.15 (4 × s, 1P). Anal. found (calcd): C, 44.92 (45.05); H, 9.49 (9.37); N, 4.69 (4.57).

[(dmpe)$_2$Mn{κ^2-Ge^{n}BuH(N^{i}PrCHN^{i}Pr)}] (10). 60.4 mg (0.12 mmol) of [(dmpe)$_2$MnH(=Ge^{n}BuH)] (**2a**) was dissolved in

5 mL of benzene. 50 mg (0.40 mmol) of diisopropylcarbodiimide was added, and the reaction mixture stirred for 2 days at room temperature. The solvent was removed *in vacuo*, and the resulting red oil was dissolved in ~1 mL of hexanes. Solid residue was removed by centrifugation, and the mother liquor was removed *in vacuo*. The resulting oil was recrystallized from a minimal amount of hexamethyldisiloxane at −30 °C to afford 28.3 mg (0.05 mmol, 37%) of [(dmpe)$_2$Mn{κ^2-Ge^{n}BuH(N^{i}PrCHN^{i}Pr)}] (**10**) as a sticky orange powder with >95% purity by NMR spectroscopy. IR (Nujol mull): ν(Ge–H) 1797 cm^{-1} (broad; calcd 1772 and 1781 cm^{-1} for the lower and higher energy diastereomers, respectively), $\nu(\mathrm{NCN})_{asym(\mathrm{bridging})}$ 1594 cm^{-1} (calcd 1600 and 1607 cm^{-1} for the lower and higher energy diastereomers, respectively). Vis: λ_{max} 459 nm. Selected NMR data for the dominant diastereomer are as follows. **^{1}H NMR (C$_6$D$_6$, 600 MHz, 298 K)**: δ 7.59 (s, 1H, NC*H*N), 5.85 (m, 1H, Ge*H*), 3.82 (hept, 1H, $^3J_{H,H}$ 6.7 Hz, C*H*Me$_2$), 3.06 (hept, 1H, $^3J_{H,H}$ 6.8 Hz, C*H*Me$_2$), 2.16, 2.02 (2 × m, 1H, CH$_2$C*H*$_2$CH$_2$CH$_3$), 1.66 (m, 2H, CH$_2$CH$_2$C*H*$_2$CH$_3$), 1.46 (d, 3H, $^2J_{H,P}$ 5.8 Hz, PC*H*$_3$), 1.44 (d, 3H, $^2J_{H,P}$ 5.6 Hz, PC*H*$_3$), 1.38 (d, 3H, $^2J_{H,P}$ 3.9 Hz, PC*H*$_3$), 1.36, 1.26 (2 × m, 1H, C*H*$_2$CH$_2$CH$_2$CH$_3$), 1.24 (m, 9H, PC*H*$_3$), 1.11 (t, 3H, $^3J_{H,H}$ 7.4 Hz, CH$_2$CH$_2$CH$_2$C*H*$_3$), 1.04 (d, 3H, $^2J_{H,P}$ 4.9 Hz, PC*H*$_3$), 0.99 (d, 3H, $^3J_{H,H}$ 6.8 Hz, CH(C*H*$_3$)$_2$), 0.86 (d, 3H, $^3J_{H,H}$ 6.5 Hz, CH(C*H*$_3$)$_2$), 0.83 (d, 3H, $^2J_{H,P}$ 4.6 Hz, PC*H*$_3$). **^{13}C{^{1}H} NMR (C$_6$D$_6$, 151 MHz, 298 K)**: δ 159.71 (s, N*C*HN), 51.49 (s, *C*HMe$_2$), 36.18 (s, CH$_2$*C*H$_2$CH$_2$CH$_3$), 29.38, 26.07 (2 × m, P*C*H$_3$), 25.62, 24.23 (2 × s, CH(*C*H$_3$)$_2$), 25.25 (s, *C*H$_2$CH$_2$CH$_2$CH$_3$), 24.09 (d, $J_{C,P}$ 9.8 Hz, P*C*H$_3$), 20.99 (d, $J_{C,P}$ 12.3 Hz, P*C*H$_3$), 20.82 (d, $J_{C,P}$ 19.6 Hz, P*C*H$_3$), 14.40 (s, CH$_2$CH$_2$CH$_2$*C*H$_3$). **^{31}P{^{1}H} NMR (C$_6$D$_6$, 243 MHz, 298 K)**: δ 77.30, 73.03, 71.68, 58.58 (4 × s, 1P). Selected NMR data for the minor diastereomer are as follows. **^{1}H NMR (C$_6$D$_6$, 600 MHz, 298 K)**: δ 7.61 (s, 1H, NC*H*N), 5.96 (t, 1H, $^3J_{H,P}$ 10.9 Hz, Ge*H*), 3.85 (hept, 1H, $^3J_{H,H}$ 6.7 Hz, C*H*Me$_2$), 3.03 (hept, 1H, $^3J_{H,H}$ 6.8 Hz, C*H*Me$_2$), 2.15, 2.01 (2 × m, 1H, CH$_2$C*H*$_2$CH$_2$CH$_3$), 1.66 (m, 2H, CH$_2$CH$_2$C*H*$_2$CH$_3$), 1.49 (d, 3H, $^2J_{H,P}$ 6.3 Hz, PC*H*$_3$), 1.42, 1.33 (2 × m, 1H, C*H*$_2$CH$_2$CH$_2$CH$_3$), 1.37 (d, 3H, $^2J_{H,P}$ 5.0 Hz, PC*H*$_3$), 1.34 (d, 3H, $^2J_{H,P}$ 6.4 Hz, PC*H*$_3$), 1.33 (d, 3H, $^2J_{H,P}$ 4.0 Hz, PC*H*$_3$), 1.24 (m, 6H, PC*H*$_3$), 1.12 (t, 3H, $^3J_{H,H}$ 7.4 Hz, CH$_2$CH$_2$CH$_2$C*H*$_3$), 1.04 (d, 3H, $^2J_{H,P}$ 4.9 Hz, PC*H*$_3$), 0.95 (d, 3H, $^3J_{H,H}$ 6.8 Hz, CH(C*H*$_3$)$_2$), 0.89 (d, 3H, $^3J_{H,H}$ 6.5 Hz, CH(C*H*$_3$)$_2$), 0.84 (d, 3H, $^2J_{H,P}$ 4.7 Hz, PC*H*$_3$). **^{13}C{^{1}H} NMR (C$_6$D$_6$, 151 MHz, 298 K)**: δ 159.64 (s, N*C*HN), 51.30 (s, *C*HMe$_2$), 36.10 (s, CH$_2$*C*H$_2$CH$_2$CH$_3$), 29.38, 26.00, 23.52 (3 × m, P*C*H$_3$), 34.61 (d of d, $J_{C,P}$ 24.4 and 15.3 Hz, P*C*H$_2$), 33.45 (d of d, $J_{C,P}$ 23.9 and 15.1 Hz, P*C*H$_2$), 31.84 (d of d, $J_{C,P}$ 22.3 and 16.6 Hz, P*C*H$_2$), 28.94 (d of d, $J_{C,P}$ 24.1 and 15.7 Hz, P*C*H$_2$), 25.25 (s, *C*H$_2$CH$_2$CH$_2$CH$_3$), 25.07, 24.63 (2 × s, CH(*C*H$_3$)$_2$), 24.90 (d, $J_{C,P}$ 16.1 Hz, P*C*H$_3$), 17.90 (d, $J_{C,P}$ 9.6 Hz, P*C*H$_3$), 14.40 (s, CH$_2$CH$_2$CH$_2$*C*H$_3$), 13.51 (d, $J_{C,P}$ 14.0 Hz, P*C*H$_3$). **^{31}P{^{1}H} NMR (C$_6$D$_6$, 243 MHz, 298 K)**: δ 75.46, 73.03, 68.61, 57.97 (4 × s, 1P). NMR environments unassigned to a specific diastereomer are as follows. **^{1}H NMR (C$_6$D$_6$, 600 MHz, 298 K)**: δ 1.49–1.98, 1.22, 0.97 (3 × m, PC*H*$_2$), 1.26, 1.22 (2 × m, CH(C*H*$_3$)$_2$). **^{13}C{^{1}H} NMR (C$_6$D$_6$, 151 MHz, 298 K)**: δ 58.61, 58.55 (2 × s, *C*HMe$_2$), 36.40 (m, P*C*H$_2$), 28.18, 28.14 (2 × s, CH$_2$CH$_2$*C*H$_2$CH$_3$), 26.92, 24.49 (2 × m, P*C*H$_3$), 25.55 (d of d, $J_{C,P}$ 17.2 and 4.9 Hz, P*C*H$_3$), 25.34, 25.25, 24.54 (3 × s, CH(*C*H$_3$)$_2$), 14.23 (d, $J_{C,P}$ 11.6 Hz, P*C*H$_3$). Anal. found (calcd): C, 44.47 (45.05); H, 9.37 (9.37); N, 4.89 (4.57).

[(dmpe)$_2$Mn{κ^2-Ge^{n}Bu(κ^1-O$_2$CH)(N^{i}PrCHN^{i}Pr)}] (11). 57.3 mg (0.12 mmol) of [(dmpe)$_2$MnH(=Ge^{n}BuH)] (**2a**) was dissolved in 5 mL of benzene. 45 mg (0.36 mmol) of diisopropylcarbodiimide was added, and the solution stirred for 2 days at room temperature to afford a bright orange solution containing **10**. The mixture was freeze/pump/thawed three times in a 50 mL bomb, placed under 1 atm of CO$_2$ at 0 °C, sealed, and warmed to room temperature. Stirring for 1 hour at room temperature resulted in an orange/red solution. The solvent was removed *in vacuo* to afford an orange powder, which was dissolved in 5 mL of hexanes. Solid residue was removed by centrifugation, and the mother liquor was maintained at −30 °C to afford 42.2 mg (0.06 mmol) of [(dmpe)$_2$Mn{κ^2-Ge^{n}Bu(κ^1-O$_2$CH)(N^{i}PrCHN^{i}Pr)}] (**11**) as X-ray quality crystals. The mother liquor was concentrated and left again at −30 °C to afford an additional 9.5 mg (0.01 mmol) of **11**, for a combined yield of 67%. IR (Nujol mull): $\nu(\mathrm{OCO})_{asym(\mathrm{terminal})}$ 1658, 1637 cm^{-1} (calcd 1646 and 1665 cm^{-1} for the lower and higher energy diastereomers, respectively), $\nu(\mathrm{NCN})_{asym(\mathrm{bridging})}$ 1589 cm^{-1} (calcd 1599 and 1603 cm^{-1} for the lower and higher energy diastereomers, respectively). Vis: λ_{max} 465 nm. Selected major diastereomer NMR data are as follows. **^{1}H NMR (C$_6$D$_6$, 500 MHz, 298 K)**: δ 8.87 (s, 1H, OC*H*O), 7.83 (s, 1H, NC*H*N), 4.44 (hept, 1H, $^3J_{H,H}$ 6.7 Hz, C*H*Me$_2$), 2.95 (hept, 1H, $^3J_{H,H}$ 6.6 Hz, C*H*Me$_2$), 2.07, 0.88 (2 × m, 1H, PC*H*$_2$), 1.96 (m, 2H, CH$_2$C*H*$_2$CH$_2$CH$_3$), 1.69 (m, 2H, PC*H*$_2$), 1.61 (d, 3H, $^2J_{H,P}$ 5.2 Hz, PC*H*$_3$), 1.60 (d, 3H, $^2J_{H,P}$ 6.1 Hz, PC*H*$_3$), 1.57 (m, 2H, CH$_2$CH$_2$C*H*$_2$CH$_3$), 1.35 (d, 3H, $^3J_{H,H}$ 6.7 Hz, CH(C*H*$_3$)$_2$), 1.33 (d, 3H, $^2J_{H,P}$ 4.7 Hz, PC*H*$_3$), 1.22 (d, 3H, $^2J_{H,P}$ 3.7 Hz, PC*H*$_3$), 1.18 (d, 3H, $^3J_{H,H}$ 6.8 Hz, CH(C*H*$_3$)$_2$), 1.15 (d, 6H, $^2J_{H,P}$ 4.0 Hz, PC*H*$_3$), 1.08 (d, 3H, $^2J_{H,P}$ 3.2 Hz, PC*H*$_3$), 1.08 (t, 3H, $^3J_{H,H}$ 7.4 Hz, CH$_2$CH$_2$CH$_2$C*H*$_3$), 0.98 (d, 3H, $^3J_{H,H}$ 6.9 Hz, CH(C*H*$_3$)$_2$), 0.78 (d, 3H, $^3J_{H,H}$ 6.6 Hz, CH(C*H*$_3$)$_2$), 0.76 (d, 3H, $^2J_{H,P}$ 4.8 Hz, PC*H*$_3$). **^{13}C{^{1}H} NMR (C$_6$D$_6$, 126 MHz, 298 K)**: δ 164.06 (s, O*C*HO), 160.23 (s, N*C*HN), 58.98 (d, $J_{C,P}$ 9.0 Hz, *C*HMe$_2$), 48.16 (s, *C*HMe$_2$), 35.81, 34.48, 31.07 (3 × m, P*C*H$_2$), 32.76 (d, $J_{C,P}$ 17.4 Hz, P*C*H$_3$), 32.38 (s, *C*H$_2$CH$_2$CH$_2$CH$_3$), 29.41 (s, CH$_2$*C*H$_2$CH$_2$CH$_3$), 27.76 (s, CH$_2$CH$_2$*C*H$_2$CH$_3$), 25.88, 25.75, 25.41, 24.08 (4 × s, CH(*C*H$_3$)$_2$), 25.15, 24.94, 23.92, 23.12, 19.40, 17.97 (6 × m, P*C*H$_3$), 14.16 (s, CH$_2$CH$_2$CH$_2$*C*H$_3$). **^{31}P{^{1}H} NMR (C$_6$D$_6$, 202 MHz, 298 K)**: δ 73.94, 60.06 (2 × s, 1P), 68.31 (m, 2P). Selected minor diastereomer NMR data are as follows. **^{1}H NMR (C$_6$D$_6$, 500 MHz, 298 K)**: δ 8.86 (s, 1H, OC*H*O), 7.77 (s, 1H, NC*H*N), 4.39 (hept, 1H, $^3J_{H,H}$ 6.8 Hz, C*H*Me$_2$), 2.93 (hept, 1H, $^3J_{H,H}$ 6.5 Hz, C*H*Me$_2$), 1.96 (m, 2H, CH$_2$C*H*$_2$CH$_2$CH$_3$), 1.57 (m, 2H, CH$_2$CH$_2$C*H*$_2$CH$_3$), 1.49 (d, 3H, $^2J_{H,P}$ 5.8 Hz, PC*H*$_3$), 1.48 (d, 3H, $^2J_{H,P}$ 4.7 Hz, PC*H*$_3$), 1.45 (d, 3H, $^2J_{H,P}$ 6.8 Hz, PC*H*$_3$), 1.32 (d, 3H, $^3J_{H,H}$ 7.0 Hz, CH(C*H*$_3$)$_2$), 1.31 (d, 3H, $^2J_{H,P}$ 4.9 Hz, PC*H*$_3$), 1.21 (d, 3H, $^2J_{H,P}$ 5.4 Hz, PC*H*$_3$), 1.18 (d, 3H, $^3J_{H,H}$ 6.7 Hz, CH(C*H*$_3$)$_2$), 1.11 (d, 3H, $^2J_{H,P}$ 3.9 Hz, PC*H*$_3$), 1.08 (t, 3H, $^3J_{H,H}$ 7.4 Hz, CH$_2$CH$_2$CH$_2$C*H*$_3$), 0.88 (d, 3H, $^3J_{H,H}$ 6.9 Hz, CH(C*H*$_3$)$_2$), 0.85 (d, 3H, $^3J_{H,H}$ 6.6 Hz, CH(C*H*$_3$)$_2$), 0.77 (d, 3H, $^2J_{H,P}$

6.0 Hz, PC$\underline{H}_3$). **^{13}C{^{1}H} NMR (C_6D_6, 126 MHz, 298 K):** δ 163.66 (s, O$\underline{C}$HO), 160.03 (s, N$\underline{C}$HN), 58.60 (d, $J_{C,P}$ 8.2 Hz, $\underline{C}$HMe$_2$), 48.19 (s, $\underline{C}$HMe$_2$), 35.81, 34.48 (2 × m, P$\underline{C}$H$_2$), 32.38 (s, $\underline{C}$H$_2$CH$_2$CH$_2$CH$_3$), 31.96, 25.15, 23.70, 23.58, 21.44, 16.61 (6 × m, P$\underline{C}$H$_3$), 29.70 (s, CH$_2\underline{C}$H$_2$CH$_2$CH$_3$), 27.76 (s, CH$_2$CH$_2\underline{C}$H$_2$CH$_3$), 25.57, 25.15, 24.40 (3 × s, CH($\underline{C}$H$_3$)$_2$), 14.13 (s, CH$_2$CH$_2$CH$_2\underline{C}$H$_3$). **^{31}P{^{1}H} NMR (C_6D_6, 202 MHz, 298 K):** δ 75.40, 69.51, 68.31, 60.06 (4 × s, 1P). NMR environments unassigned to a specific diastereomer are as follows. **^{1}H NMR (C_6D_6, 500 MHz, 298 K):** δ 1.84, 1.56 (2 × m, C$\underline{H}_2$CH$_2$CH$_2$CH$_3$). Anal. found (calcd): C, 43.80 (43.86); H, 8.84 (8.74); N, 4.22 (4.26).

Monitoring the reaction of [(dmpe)$_2$Mn{κ^2-SiPhH(N^{i}PrCHN^{i}Pr)}] with CO_2 to form [(dmpe)$_2$Mn{κ^2-SiPh(κ^1-O$_2$CH)(N^{i}PrCHN^{i}Pr)}] (12). 14.7 mg (0.02 mmol) of [(dmpe)$_2$Mn{κ^2-SiPhH(N^{i}PrCHN^{i}Pr)}] was dissolved in approx. 0.6 mL of C_6D_6, and the solution placed in a J-young NMR tube. The mixture was freeze/pump/thawed three times, and placed under 1 atm of CO_2 at 0 °C, sealed, and warmed to room temperature. The reaction mixture was left at room temperature and monitored by NMR spectroscopy periodically. X-ray quality crystals were obtained by removing the solvent *in vacuo* and recrystallization from a dilute solution in hexanes at −30 °C. Selected NMR data for the major diastereomer are as follows. **^{1}H NMR (C_6D_6, 600 MHz, 298 K):** δ 8.72 (s, 1H, OC$\underline{H}$O), 7.79 (d, 2H, $^3J_{H,H}$ 6.8 Hz, *o*-Ph), 7.77 (s, 1H, NC$\underline{H}$N), 7.26 (t, 2H, $^3J_{H,H}$ 7.4 Hz, *m*-Ph), 7.19 (t, 1H, $^3J_{H,H}$ 7.1 Hz, *p*-Ph), 3.39, 2.91 (2 × hept., 1H, $^3J_{H,H}$ 6.6 Hz, C$\underline{H}$Me$_2$), 2.42, 1.77 (2 × m, 1H, PC$\underline{H}_2$), 1.61, (d, 3H, $^2J_{H,P}$ 6.6 Hz, PC$\underline{H}_3$), 1.61 (m, 2H, PC$\underline{H}_2$), 1.38 (d, 3H, $^2J_{H,P}$ 5.4 Hz, PC$\underline{H}_3$), 1.29, 0.67 (2 × d, 3H, $^2J_{H,P}$ 4.4 Hz, PC$\underline{H}_3$), 1.21 (d, 3H, $^2J_{H,P}$ 3.0 Hz, PC$\underline{H}_3$), 1.18 (d, 3H, $^2J_{H,P}$ 4.8 Hz, PC$\underline{H}_3$), 1.10 (d, 3H, $^2J_{H,P}$ 4.2 Hz, PC$\underline{H}_3$), 1.05 (d, 3H, $^3J_{H,H}$ 6.8 Hz, CH(C$\underline{H}_3$)$_2$), 1.03, 0.93, 0.87 (3 × d, 3H, $^3J_{H,H}$ 6.6 Hz, CH(C$\underline{H}_3$)$_2$), 0.74 (m, 1H, PC$\underline{H}_2$), 0.74 (d, 3H, $^2J_{H,P}$ 5.5 Hz, PC$\underline{H}_3$). **^{13}C{^{1}H} NMR (C_6D_6, 151 MHz, 298 K):** δ 161.14 (s, O$\underline{C}$HO), 160.00 (s, N$\underline{C}$HN), 148.75 (s, *i*-Ph), 136.20 (s, *o*-Ph), 127.33, 127.31 (2 × s, *m*-Ph and *p*-Ph), 59.84 (d, $J_{C,P}$ 9.7 Hz, $\underline{C}$HMe$_2$), 48.45 (s, $\underline{C}$HMe$_2$), 35.20 (m, P$\underline{C}$H$_2$), 31.73 (d, $J_{C,P}$ 17.7 Hz, P$\underline{C}$H$_3$), 30.22 (d of d, $J_{C,P}$ 26.3 and 15.4 Hz, P$\underline{C}$H$_2$), 26.84 (d, $J_{C,P}$ 10.1 Hz, P$\underline{C}$H$_3$), 25.87 (d, $J_{C,P}$ 15.5 Hz, P$\underline{C}$H$_3$), 25.43, 24.99, 24.90, 24.54 (4 × s, CH($\underline{C}$H$_3$)$_2$), 24.11 (d, $J_{C,P}$ 8.4 Hz, P$\underline{C}$H$_3$), 23.82 (m, P$\underline{C}$H$_3$), 23.06 (d, $J_{C,P}$ 20.0 Hz, P$\underline{C}$H$_3$), 19.11 (d of d, $J_{C,P}$ 9.4 and 4.8 Hz, P$\underline{C}$H$_3$), 17.61 (d, $J_{C,P}$ 15.5 Hz, P$\underline{C}$H$_3$). **^{29}Si NMR (data from ^{29}Si–^{1}H HMBC in C_6D_6, 99 MHz, 298 K):** δ 98.0. **^{31}P{^{1}H} NMR (C_6D_6, 243 MHz, 298 K):** δ 72.01 (s, 2P), 67.09, 53.47 (2 × s, 1P). Selected NMR data for the minor diastereomer are as follows. **^{1}H NMR (C_6D_6, 600 MHz, 298 K):** δ 8.64 (s, 1H, OC$\underline{H}$O), 7.85 (d, 2H, $^3J_{H,H}$ 6.8 Hz, *o*-Ph), 7.81 (m, 1H, NC$\underline{H}$N), 7.27 (t, 2H, $^3J_{H,H}$ 7.2 Hz, *m*-Ph), 7.18 (t, 1H, $^3J_{H,H}$ 7.3 Hz, *p*-Ph), 3.39 (hept., 1H, $^3J_{H,H}$ 6.6 Hz, C$\underline{H}$Me$_2$), 3.01 (hept., 1H, $^3J_{H,H}$ 6.7 Hz, C$\underline{H}$Me$_2$), 1.77 (m, 1H, PC$\underline{H}_2$), 1.75 (d, 3H, $^2J_{H,P}$ 6.4 Hz, PC$\underline{H}_3$), 1.43 (d, 3H, $^2J_{H,P}$ 5.5 Hz, PC$\underline{H}_3$), 1.38, 1.17 (2 × m, 6H, PC$\underline{H}_3$), 1.14 (d, 3H, $^2J_{H,P}$ 3.0 Hz, PC$\underline{H}_3$), 1.60 (d, 3H, $^3J_{H,H}$ 6.8 Hz, CH(C$\underline{H}_3$)$_2$), 1.00, 0.93, 0.87 (3 × d, 3H, $^3J_{H,H}$ 6.6 Hz, CH(C$\underline{H}_3$)$_2$), 0.97 (m, 1H, PC$\underline{H}_2$), 0.74 (d, 3H, $^2J_{H,P}$ 4.3 Hz, PC$\underline{H}_3$), 0.74 (m, 1H, PC$\underline{H}_2$). **^{13}C{^{1}H} NMR (C_6D_6, 151 MHz, 298 K):** δ 160.98 (s, O$\underline{C}$HO), 160.37 (s, N$\underline{C}$HN), 148.75 (s, *i*-Ph), 136.44 (s, *o*-Ph), 59.48 (d, $J_{C,P}$ 8.9 Hz, $\underline{C}$HMe$_2$), 48.55 (s, $\underline{C}$HMe$_2$), 35.20 (m, P$\underline{C}$H$_2$), 32.53 (d, of d, $J_{C,P}$ 24.4 and 15.4 Hz, P$\underline{C}$H$_2$), 30.64 (d, $J_{C,P}$ 17.9 Hz, P$\underline{C}$H$_3$), 26.52, 25.18, 23.82, 15.75 (4 × m, P$\underline{C}$H$_3$), 26.06 (d of d, $J_{C,P}$ 17.1 and 4.2 Hz, P$\underline{C}$H$_3$), 25.73, 24.96, 24.65, 24.47 (4 × s, CH($\underline{C}$H$_3$)$_2$), 20.63 (d, $J_{C,P}$ 12.8 Hz, P$\underline{C}$H$_3$). **^{29}Si NMR (data from ^{29}Si–^{1}H HMBC in C_6D_6, 99 MHz, 298 K):** δ 97.1. **^{31}P{^{1}H} NMR (C_6D_6, 243 MHz, 298 K):** δ 72.01, 69.44, 66.57, 55.14 (4 × s, 1P). NMR environments unassigned to a specific diastereomer are as follows. **^{1}H NMR (C_6D_6, 600 MHz, 298 K):** δ 1.27–1.42 (m, PC$\underline{H}_2$).

[(dmpe)$_2$Mn(GeH$_2$^{n}Bu)(CN^{t}Bu)] (13a). 16.2 mg (0.03 mmol) of [(dmpe)$_2$MnH(=GeEt$_2$)] (**1b**) and 24.6 mg (0.19 mmol) of H$_3$Ge^{n}Bu were dissolved in approx. 0.6 mL of C_6D_6 and placed in a J-young tube. After allowing the reactions to sit at room temperature for 1.75 hours, 9.2 mg (0.11 mmol) of *tert*-butyl isonitrile was added, and the yellow reaction mixture was analyzed *in situ* by NMR spectroscopy, indicating complete conversion to **13a** within 15 minutes (as a 5.6 : 1 mixture of ***cis*-13a** : ***trans*-13a**). After sitting overnight at room temperature, the solvent and free hydrogermanes were removed *in vacuo*, and the resulting green solid was dissolved in approx. 0.6 mL of C_6D_6 to afford a clear yellow solution which was analyzed *in situ* by NMR spectroscopy (as an 8 : 1 mixture of ***cis*-13a** : ***trans*-13a**). X-ray quality crystals of ***cis*-13a** were obtained by removal of the solvent *in vacuo* followed by recrystallization from a concentrated solution of hexamethyldisiloxane at −30 °C. ***cis* isomer: ^{1}H NMR (C_6D_6, 500 MHz, 298 K):** δ 3.73 3.52 (2 × m, 1H, Ge$\underline{H}$), 2.19 (quin., 2H, $^3J_{H,H}$ 7.7 Hz, CH$_2$C$\underline{H}_2$CH$_2$CH$_3$), 1.33–1.80 (m, 5H, PC$\underline{H}_2$), 1.76 (sext., 2H, $^3J_{H,H}$ 7.4 Hz, CH$_2$CH$_2$C$\underline{H}_2$CH$_3$), 1.63, 1.58 (d, 3H, $^2J_{H,P}$ 6.9 Hz, PC$\underline{H}_3$), 1.31 (m, 2H, C$\underline{H}_2$CH$_2$CH$_2$CH$_3$), 1.30, 1.28 (2 × d, 3H, $^2J_{H,P}$ 6.1 Hz, PC$\underline{H}_3$), 1.23 (s, 9H, C(C$\underline{H}_3$)$_3$), 1.20 (d, 3H, $^2J_{H,P}$ 6.2 Hz, PC$\underline{H}_3$), 1.17 (d, 3H, $^2J_{H,P}$ 6.0 Hz, PC$\underline{H}_3$), 1.14 (t, 3H, $^3J_{H,H}$ 7.4 Hz, CH$_2$CH$_2$CH$_2$C$\underline{H}_3$), 0.79–1.09 (m, 3H, PC$\underline{H}_2$), 1.07, 0.84 (2 × d, 3H, $^2J_{H,P}$ 4.8 Hz, PC$\underline{H}_3$). **^{13}C{^{1}H} NMR (C_6D_6, 126 MHz, 298 K):** δ 54.63 (s, $\underline{C}$(CH$_3$)$_3$), 37.26 (s, CH$_2\underline{C}$H$_2$CH$_2$CH$_3$), 34.76 (app. t of d, $J_{C,P}$ 20.9 and 4.9 Hz, P$\underline{C}$H$_2$), 33.70 (app. t of d, $J_{C,P}$ 24.1 and 8.6 Hz, P$\underline{C}$H$_2$), 31.98 (s, C($\underline{C}$H$_3$)$_3$), 31.78 (m, P$\underline{C}$H$_2$), 30.06 (app. t, $J_{C,P}$ 19.2 Hz, P$\underline{C}$H$_2$), 27.61 (s, CH$_2$CH$_2\underline{C}$H$_2$CH$_3$), 23.82 (d of d, $J_{C,P}$ 13.2 and 5.5 Hz, P$\underline{C}$H$_3$), 23.55 (d, $J_{C,P}$ 10.5 Hz, P$\underline{C}$H$_3$), 23.17 (d, $J_{C,P}$ 9.0 Hz, P$\underline{C}$H$_3$), 22.08 (d of d, $J_{C,P}$ 18.5 and 6.1 Hz, P$\underline{C}$H$_3$), 20.10 (d of d, $J_{C,P}$ 11.5 and 4.2 Hz, P$\underline{C}$H$_3$), 18.08–18.65 (m, P$\underline{C}$H$_3$), 18.43 (s, $\underline{C}$H$_2$CH$_2$CH$_2$CH$_3$), 14.65 (s, CH$_2$CH$_2$CH$_2\underline{C}$H$_3$). **^{31}P{^{1}H} NMR (C_6D_6, 202 MHz, 298 K):** δ 64–83 (m, 3P), 57.1 (br. s, 1P). ***trans* isomer: ^{1}H NMR (C_6D_6, 500 MHz, 298 K):** δ 3.26 (m, 2H, Ge$\underline{H}$), 2.05 (quin., 2H, $^3J_{H,H}$ 7.7 Hz, CH$_2$C$\underline{H}_2$CH$_2$CH$_3$), 1.66 (sext., 2H, $^3J_{H,H}$ 7.4 Hz, CH$_2$CH$_2$C$\underline{H}_2$CH$_3$), 1.66, 1.39 (2 × m, 4H, PC$\underline{H}_2$), 1.51, 1.27 (2 × s, 12H, PC$\underline{H}_3$), 1.08 (t, 3H, $^3J_{H,H}$ 7.4 Hz, CH$_2$CH$_2$CH$_2$C$\underline{H}_3$), 1.05 (s, 9H, C(C$\underline{H}_3$)$_3$), 0.89 (m, 2H, C$\underline{H}_2$CH$_2$CH$_2$CH$_3$). **^{13}C{^{1}H} NMR (C_6D_6, 126 MHz, 298 K):** δ 54.27 (s, $\underline{C}$(CH$_3$)$_3$), 38.51 (s, CH$_2\underline{C}$H$_2$CH$_2$CH$_3$), 32.26 (m, P$\underline{C}$H$_2$), 31.85 (s, C($\underline{C}$H$_3$)$_3$), 27.65 (s, CH$_2$CH$_2\underline{C}$H$_2$CH$_3$), 21.83, 20.20 (2 × m, P$\underline{C}$H$_3$), 20.97 (s, $\underline{C}$H$_2$CH$_2$CH$_2$CH$_3$), 14.57 (s, CH$_2$CH$_2$CH$_2\underline{C}$H$_3$). **^{31}P{^{1}H} NMR (C_6D_6, 202 MHz, 298 K):** δ 73.49 (s).

[(dmpe)$_2$Mn(GeH$_2$Ph)(CN^{t}Bu)] (13b). 59.5 mg (0.12 mmol) of [(dmpe)$_2$MnH(=GeEt$_2$)] (**1b**) was dissolved in 5 mL benzene and placed in a 50 mL bomb. 85 mg (0.56 mmol) of H$_3$GePh was then added, and the reaction stirred in the dark at room temperature for 1.5 hours. 117.6 mg (1.41 mmol) of *tert*-butyl isonitrile was then added, and the reaction mixture was stirred at room temperature in the dark overnight. Solvent was then removed *in vacuo*, and the resulting powder was recrystallized from hexanes at −30 °C to afford 30.2 mg (0.05 mmol, 42%) of [(dmpe)$_2$Mn(GeH$_2$Ph)(CN^{t}Bu)] (**13b**; with a 0.5 : 1 ratio of ***cis*-13b : *trans*-13b**) as a yellow powder with ~95% purity by ^{1}H NMR spectroscopy. An additional 2.3 mg (0.004 mmol, 3%) of analytically pure **13b** was isolated by dissolving the residue (which did not dissolve in the hexanes used for the initial crystallization) in 0.2 mL of toluene and cooling to −30 °C. X-ray quality crystals of ***cis*-13b** were obtained by recrystallization from a solution of toluene layered with pentane at −30 °C. X-ray quality crystals of ***trans*-13b** were obtained by dissolving approx. 10 mg of isolated [(dmpe)$_2$Mn(GeH$_2$Ph)(CN^{t}Bu)] (**13b**) in approx. 0.6 mL of C$_6$D$_6$, heating in a sealed J-Young tube at 90–95 °C for 6 days (resulting in a *cis* : *trans* ratio of 8 : 92), removing the solvent *in vacuo*, washing the resulting solid with hexanes, and finally recrystallizing from toluene layered with hexamethyldisiloxane at −30 °C. **Selected NMR data for the *cis* isomer: ^{1}H NMR (C$_6$D$_6$, 500 MHz, 298 K):** δ 8.15 (d of d, 2H, $^3J_{H,H}$ 7.9 Hz, $^4J_{H,H}$ 1.3 Hz, *o*-Ph), 7.29 (t, 2H, $^3J_{H,H}$ 7.4 Hz, *m*-Ph), 7.20 (*p*-Ph),¶ 4.72 (d of d, 1H, $^3J_{H,P}$ 14.2 Hz and 7.3 Hz, GeH), 4.51 (q, 1H, $^3J_{H,P}$ 6.4 Hz, GeH), 1.56–1.80 (m, 2H, PCH$_2$), 1.69 (d, 3H, $^2J_{H,P}$ 7.0 Hz, PCH$_3$), 1.60 (d, 3H, $^2J_{H,P}$ 6.9 Hz, PCH$_3$), 1.35, 1.29, 1.16 (3 × d, 3H, $^2J_{H,P}$ 6.1 Hz, PCH$_3$), 1.26–1.49 (m, 3H, PCH$_2$), 1.19 (d, 3H, $^2J_{H,P}$ 6.2 Hz, PCH$_3$), 1.03–1.13 (m, 2H, PCH$_2$), 1.02 (d, 3H, $^2J_{H,P}$ 5.1 Hz, PCH$_3$), 1.01 (s, 9H, C(CH$_3$)$_3$), 0.92 (m, 1H, PCH$_2$), 0.83 (d, 3H, $^2J_{H,P}$ 4.8 Hz, PCH$_3$). **^{13}C{^{1}H} NMR (C$_6$D$_6$, 126 MHz, 298 K):** δ 153.73 (d, $^3J_{C,P}$ 5.2 Hz, *i*-Ph), 137.63 (s, *o*-Ph), 127.09 (s, *m*-Ph), 125.35 (s, *p*-Ph), 54.71 (s, CMe$_3$), 34.54 (t of d, $J_{C,P}$ 20.4 and 5.9 Hz, PCH$_2$), 33.22 (t of d, $J_{C,P}$ 23.8 Hz and 8.5 Hz, PCH$_2$), 32.19 (m, PCH$_2$), 30.65 (app. t, $J_{C,P}$ 19.4 Hz, PCH$_2$), 23.72 (d of d, $J_{C,P}$ 10.9 and 2.8 Hz, PCH$_3$), 23.39 (d of m, $J_{C,P}$ 14.8 Hz, PCH$_3$), 23.05 (d, $J_{C,P}$ 9.0 Hz, PCH$_3$), 22.00 (d of d, $J_{C,P}$ 18.3 and 6.4 Hz, PCH$_3$), 20.30 (d of d, $J_{C,P}$ 12.2 and 4.3 Hz, PCH$_3$), 20.00, 19.89 (2 × m, PCH$_3$), 18.77 (d of d, $J_{C,P}$ 18.2 and 4.6 Hz, PCH$_3$). **^{31}P{^{1}H} NMR (C$_6$D$_6$, 202 MHz, 298 K):** δ 67–78 (m, 3P), 56.84 (br. s, 1P). **Selected NMR data for the *trans* isomer: ^{1}H NMR (C$_6$D$_6$, 500 MHz, 298 K):** δ 7.88 (d of d, 2H $^3J_{H,H}$ 7.8 Hz, $^4J_{H,H}$ 1.4 Hz, *o*-Ph), 7.23 (t, 2H, $^3J_{H,H}$ 7.1 Hz, *m*-Ph), 7.16 (*p*-Ph),¶ 4.25 (quin., 2H, $^3J_{H,P}$ 7.1 Hz, GeH), 1.71, 1.37 (2 × m, 4H, PCH$_2$), 1.45, 1.23 (2 × s, 12H, PCH$_3$), 1.01 (s, 9H, C(CH$_3$)$_3$). **^{13}C{^{1}H} NMR (C$_6$D$_6$, 126 MHz, 298 K):** δ 155.75 (s, *i*-Ph), 136.72 (s, *o*-Ph), 127.43 (s, *m*-Ph), 125.43 (s, *p*-Ph), 54.41 (s, CMe$_3$), 32.19 (m, PCH$_2$), 21.45, 19.98 (2 × m, PCH$_3$). **^{31}P{^{1}H} NMR (C$_6$D$_6$, 202 MHz, 298 K):** δ 72.08 (s). NMR environments unassigned to a specific isomer are as follows. **^{13}C{^{1}H} NMR (C$_6$D$_6$, 126 MHz, 298 K):** δ 31.73, 31.67 (2 × s, C(CH$_3$)$_3$). Anal. found (calcd): C, 46.69 (46.81); H, 8.08 (8.20); N, 2.15 (2.37).

Additional spectroscopic data for [(dmpe)$_2$MnH(=GeRR′)] (1a: R = R′ = Ph, 1b: R = R′ = Et, 2a: R = ^{n}Bu and R′ = H). Vis: λ_{max} 468 nm (**1a**), λ_{max} 431 nm (**1b**), and λ_{max} 432 nm (**2a**). IR (Nujol mull): **1a:** ν(Mn–H) 1709 cm^{-1} (calcd 1800 cm^{-1}), **1b:** ν(Mn–H) 1685 cm^{-1} (calcd 1772 cm^{-1}), **2a:** ν(H–MnGe–H)$_{asym}$ 1688 cm^{-1} (calcd 1724 cm^{-1}); ν(H–MnGe–H)$_{sym}$ 1766 cm^{-1} (calcd 1773 cm^{-1}).

Conflicts of interest

There are no conflicts to declare.

Data availability

Data supporting this article is included in the SI.

Supplementary information: general experimental information, discussion of alternative mechanisms, selected NMR, IR, and UV-Vis spectra, SCD data, and DFT results. See DOI: https://doi.org/10.1039/d5dt01701g.

CCDC 2473080–2473088 (**6**, **7**, **8**, **9a**, **11**, **12**, ***cis*-13a**, ***cis*-13b**, and ***trans*-13b**) contain the supplementary crystallographic data for this paper.[64a–i]

Acknowledgements

D. J. H. E. thanks NSERC of Canada for a Discovery Grant and Dr Yurij Mozharivskyj for access to his X-ray diffractometer.

References

1 T. Sakakura, J.-C. Choi and H. Yasuda, *Chem. Rev.*, 2007, **107**, 2365–2387.
2 M. Cokoja, C. Bruckmeier, B. Rieger, W. A. Herrmann and F. E. Kühn, *Angew. Chem., Int. Ed.*, 2011, **50**, 8510–8537.
3 I. Omae, *Coord. Chem. Rev.*, 2012, **256**, 1384–1405.
4 M. Hölscher, C. Guertler, W. Keim, T. E. Müller, M. Peters and W. Leitner, *Z. Naturforsch., B: J. Chem. Sci.*, 2012, **67**, 961–975.
5 M. Aresta, A. Dibenedetto and E. Quaranta, *J. Catal.*, 2016, **343**, 2–45.
6 Y. Li, X. Cui, K. Dong, K. Junge and M. Beller, *ACS Catal.*, 2017, **7**, 1077–1086.
7 D. H. Gibson, *Chem. Rev.*, 1996, **96**, 2063–2095.
8 X. Yin and J. R. Moss, *Coord. Chem. Rev.*, 1999, **181**, 27–59.
9 T. Fan, X. Chen and Z. Lin, *Chem. Commun.*, 2012, **48**, 10808–10828.
10 A. Paparo and J. Okuda, *Coord. Chem. Rev.*, 2017, **334**, 136–149.
11 K. A. Grice, *Coord. Chem. Rev.*, 2017, **336**, 78–95.
12 A. Jana, D. Ghoshal, H. W. Roesky, I. Objartel, G. Schwab and D. Stalke, *J. Am. Chem. Soc.*, 2009, **131**, 1288–1293.
13 S. L. Choong, W. D. Woodul, C. Schenk, A. Stasch, A. F. Richards and C. Jones, *Organometallics*, 2011, **30**, 5543–5550.

14 G. Tan, W. Wang, B. Blom and M. Driess, *Dalton Trans.*, 2014, **43**, 6006–6011.
15 L. R. Sita, J. R. Babcock and R. Xi, *J. Am. Chem. Soc.*, 1996, **118**, 10912–10913.
16 L. Groll, J. A. Kelly and S. Inoue, *Chem. – Asian J.*, 2024, **19**, e202300941.
17 T. J. Hadlington, C. E. Kefalidis, L. Maron and C. Jones, *ACS Catal.*, 2017, **7**, 1853–1859.
18 N. Villegas-Escobar, H. F. Schaefer III and A. Toro-Labbé, *J. Phys. Chem. A*, 2020, **124**, 1121–1133.
19 A. Bücker, C. Wölper and S. Schulz, *Polyhedron*, 2024, **247**, 116702.
20 J. Lundahl, L. E. English, J. S. Ward and P. Vasko, *Eur. J. Inorg. Chem.*, 2025, **28**, e202500116.
21 K. E. Litz, K. Henderson, R. W. Gourley and M. M. B. Holl, *Organometallics*, 1995, **14**, 5008–5010.
22 P. Mahawar, T. Rajeshkumar, L. Maron, T. P. Spaniol and J. Okuda, *Chem. – Eur. J.*, 2023, **29**, e202301496.
23 T. J. Hadlington, *Chem. Soc. Rev.*, 2024, **53**, 9738–9831.
24 H. Hashimoto, T. Tsubota, T. Fukuda and H. Tobita, *Chem. Lett.*, 2009, **38**, 1196–1197.
25 T. P. Dhungana, H. Hashimoto and H. Tobita, *Dalton Trans.*, 2017, **46**, 8167–8179.
26 H. Sakaba, Y. Arai, K. Suganuma and E. Kwon, *Organometallics*, 2013, **32**, 5038–5046.
27 T. P. Dhungana, H. Hashimoto, M. Ray and H. Tobita, *Organometallics*, 2020, **39**, 4350–4361.
28 H. Hashimoto, T. Fukuda and H. Tobita, *New J. Chem.*, 2010, **34**, 1723–1730.
29 H. Hashimoto, T. Fukuda, H. Tobita, M. Ray and S. Sakaki, *Angew. Chem., Int. Ed.*, 2012, **51**, 2930.
30 T. Chen, W. Hunks, P. S. Chen, G. T. Stauf, T. M. Cameron, C. Xu, A. G. DiPasquale and A. L. Rheingold, *Eur. J. Inorg. Chem.*, 2009, **2009**, 2047–2049.
31 J. S. Price, I. Vargas-Baca, D. J. H. Emslie and J. F. Britten, *Dalton Trans.*, 2023, **52**, 14880–14895.
32 J. S. Price, D. J. H. Emslie and J. F. Britten, *Angew. Chem., Int. Ed.*, 2017, **56**, 6223–6227.
33 J. S. Price, D. J. H. Emslie, I. Vargas-Baca and J. F. Britten, *Organometallics*, 2018, **37**, 3010–3023.
34 J. S. Price and D. J. H. Emslie, *Chem. Sci.*, 2019, **10**, 10853–10869.
35 J. S. Price, D. J. H. Emslie and B. Berno, *Organometallics*, 2019, **38**, 2347–2362.
36 J. S. Price and D. J. H. Emslie, *Organometallics*, 2020, **39**, 4618–4628.
37 N. J. Mosey, K. M. Baines and T. K. Woo, *J. Am. Chem. Soc.*, 2002, **124**, 13306–13321.
38 C. Perthuisot, M. Fan and W. D. Jones, *Organometallics*, 1992, **11**, 3622–3629.
39 M. E. Fasulo and T. D. Tilley, *Chem. Commun.*, 2012, **48**, 7690–7692.
40 P. B. Glaser and T. D. Tilley, *J. Am. Chem. Soc.*, 2003, **125**, 13640–13641.
41 E. Calimano and T. D. Tilley, *J. Am. Chem. Soc.*, 2008, **130**, 9226–9227.
42 W. R. Cullen, F. W. B. Einstein, R. K. Pomeroy and P. L. Vogel, *Inorg. Chem.*, 1975, **14**, 3017–3020.
43 W. Gäde and E. Weiss, *Chem. Ber.*, 1981, **114**, 2399–2404.
44 B. Schiemenz and G. Huttner, *Chem. Ber.*, 1994, **127**, 2129–2133.
45 G. Albertin, S. Antoniutti and J. Castro, *J. Organomet. Chem.*, 2012, **696**, 4191–4201.
46 S. Wolf, S. Wei, W. Klopper, S. Dehnen and C. Feldmann, *Inorg. Chem.*, 2020, **59**, 12895–12902.
47 B. T. Kilbourn, T. L. Blundell and H. M. Powell, *Chem. Commun.*, 1965, 444–445.
48 F. Carré, G. Cerveau, E. Colomer and R. J. P. Corriu, *J. Organomet. Chem.*, 1982, **229**, 257–273.
49 D. J. Brauer and R. Eujen, *Organometallics*, 1983, **2**, 263–267.
50 J. A. Cabeza, P. García-Álvarez, R. Gobetto, L. González-Álvarez, C. Nervi, E. Pérez-Carreño and D. Polo, *Organometallics*, 2016, **35**, 1761–1770.
51 D. Lei, M. J. Hampden-Smith, J. W. Garvey and J. C. Huffman, *J. Chem. Soc., Dalton Trans.*, 1991, 2449–2457.
52 R. Y. Kong, J. B. Parry, G. R. Anello, M. E. Ong and K. M. Lancaster, *J. Am. Chem. Soc.*, 2023, **145**, 24136–24144.
53 Q. Zhu, J. C. Fettinger and P. P. Power, *Dalton Trans.*, 2021, **50**, 12555–12562.
54 M. L. Buil, J. A. Cabeza, M. A. Esteruelas, S. Izquierdo, C. J. Laglera-Gándara, A. I. Nicasio and E. Oñate, *Inorg. Chem.*, 2021, **60**, 16860–16870.
55 C. R. Groom, I. J. Bruno, M. P. Lightfoot and S. C. Ward, *Acta Crystallogr., Sect. B: Struct. Sci., Cryst. Eng. Mater.*, 2016, **72**, 171–179.
56 Characteristic Bond Lengths in Free Molecules, in *CRC Handbook of Chemistry and Physics*, ed. J. R. Rumble, CRC Press/Taylor & Francis, Boca Raton, FL, 106th edn, 2025.
57 F. M. Bickelhaupt and E. J. Baerends, in *Rev. Comput. Chem*, ed. D. B. Boyd and K. B. Lipkowitz, Wiley-VCH, New York, 2000, pp. 1–86.
58 T. Ziegler and A. Rauk, *Inorg. Chem.*, 1979, **18**, 1755–1759.
59 T. Ziegler and A. Rauk, *Inorg. Chem.*, 1979, **18**, 1558–1565.
60 D. G. Gilheany, *Chem. Rev.*, 1994, **94**, 1339–1374.
61 H. Jacobsen, H. B. Kraatz, T. Ziegler and P. M. Boorman, *J. Am. Chem. Soc.*, 1992, **114**, 7851–7860.
62 H. B. Kraatz, H. Jacobsen, T. Ziegler and P. M. Boorman, *Organometallics*, 1993, **12**, 76–80.
63 J. S. Price and D. J. H. Emslie, *Dalton Trans.*, 2025, **54**, 9949–9968.
64 (*a*) J. S. Price and D. J. H. Emslie, CCDC 2473080: Experimental Crystal Structure Determination, 2025, DOI: **10.5517/ccdc.csd.cc2p0fsy**; (*b*) J. S. Price and D. J. H. Emslie, CCDC 2473081: Experimental Crystal Structure Determination, 2025, DOI: **10.5517/ccdc.csd.cc2p0ftz**; (*c*) J. S. Price and D. J. H. Emslie, CCDC 2473082: Experimental Crystal Structure Determination, 2025, DOI: **10.5517/ccdc.csd.cc2p0fv0**; (*d*) J. S. Price and D. J. H. Emslie, CCDC 2473083: Experimental Crystal

Structure Determination, 2025, DOI: 10.5517/ccdc.csd.cc2p0fw1; (*e*) J. S. Price and D. J. H. Emslie, CCDC 2473084: Experimental Crystal Structure Determination, 2025, DOI: 10.5517/ccdc.csd.cc2p0fx2; (*f*) J. S. Price and D. J. H. Emslie, CCDC 2473085: Experimental Crystal Structure Determination, 2025, DOI: 10.5517/ccdc.csd.cc2p0fy3; (*g*) J. S. Price and D. J. H. Emslie, CCDC 2473086: Experimental Crystal Structure Determination, 2025, DOI: 10.5517/ccdc.csd.cc2p0fz4; (*h*) J. S. Price and D. J. H. Emslie, CCDC 2473087: Experimental Crystal Structure Determination, 2025, DOI: 10.5517/ccdc.csd.cc2p0g06; (*i*) J. S. Price and D. J. H. Emslie, CCDC 2473088: Experimental Crystal Structure Determination, 2025, DOI: 10.5517/ccdc.csd.cc2p0g17.